Trabajo de grado

Departamento de Física (3146)

Facultad de Ciencias Naturales y Exactas

Grupo QuanTIC

Universidad del Valle

The anisotropic Bose-Hubbard dimer in the mean field approximation

Modelo de Bose-Hubbard para un pozo anisotrópico de dos sitios en la aproximación de campo medio

By:
Isabella Becerra Arbeláez

Supervisor:
Javier Madroñero Pabón

Co-supervisor:
William Esteban Salazar Estrada

Santiago de Cali, 7 de marzo del 2025

Contents

Resumen

En este proyecto se estudia el sistema formado por dos condensados de Bose-Einstein acoplados, conocido también como juntura bosónica de Josephson. Se usa un modelo de pozo doble para atrapar los átomos ultrafríos y se presta especial atención al caso poco estudiado en la literatura de pozos asimétricos. Para ello se hace una breve introducción a los condensados de Bose-Einstein y su relación con redes ópticas. Se describe también el modelo de Bose-Hubbard restringido a dos pozos y se considera un número grande de partículas que permite hacer uso de la aproximación semiclásica de campo medio. Al introducir la anisotropía en este sistema, se encuentra que hay un rompimiento se simetría en el espacio de fase, que puede ser interpretado como un proceso disipativo que emerge en la dinámica semiclásica, aunque el flujo total de partículas se conserva. Adicionalmente, se estudia este mismo sistema usando el formalismo de espín considerando un número grande de bosones. Bajo este enfoque, la anisotropía afecta a el sistema de la misma forma como un efecto Zeeman, donde el dímero se comporta como un modelo de espín total $N/2$ en presencia de un campo magnético externo proporcional a Δ. Se estudian los valores esperados de las componentes de espín y sus varianzas, en especial para $\hat{S}_z$, que por definición representa la diferencia de partículas para ambos pozos y depende fuertemente de la anisotropía. Las fluctuaciones cuánticas para $\hat{S}_x$, $\hat{S}_y$, y $\hat{S}_z$ disminuyen cuando el número de partículas aumenta, particularmente como $\propto 1/N$, sugiriendo que $\hat{S}_x$, $\hat{S}_y$, y $\hat{S}_z$ se vuelva más localizado cuánticamente cerca al límite semiclásico.

Palabras clave: átomos ultrafríos, redes ópticas, Juntura bosónica de Josephson, dímero, condensado de Bose-Einstein.

Abstract

This project studies the system formed by two coupled Bose-Einstein condensates, also known as the bosonic Josephson junction. A double-well model is used to trap the ultracold atoms, and special attention is paid to the understudied case of asymmetric wells. A brief introduction to Bose-Einstein condensates and their relationship to optical lattices is provided. The Bose-Hubbard model restricted to two wells is also described, and a large number of particles is considered, allowing for the use of the semiclassical mean-field approximation. By introducing anisotropy into this system, a symmetry breaking in phase space is found, which can be interpreted as a dissipative process emerging in semiclassical dynamics, although the total particle flux is conserved. Additionally, this same system is studied using the spin formalism considering a large number of bosons. Under this approach, the anisotropy affects the system in the same way as a Zeeman effect, where the dimer behaves as an $N/2$ spin model in the presence of an external magnetic field proportional to Δ. The expectation values of the spin components and their variances are studied, especially for $\hat{S}_z$, which by definition represents the difference of particles for both wells and depends strongly on the anisotropy. The quantum fluctuations for $\hat{S}_x$, $\hat{S}_y$, and $\hat{S}_z$ decrease with increasing particle number, particularly as $\propto 1/N$, suggesting that $\hat{S}_x$, $\hat{S}_y$, and $\hat{S}_z$ becomes more quantum localized near the semiclassical limit.

Keywords: ultracold atoms, optical lattices, Josephson bosonic junction, dimer, Bose-Einstein condensate.

Agradecimientos

Quiero agradecerle a Dios por escucharme y bendecirme siempre, incluso por las pruebas, porque me han hecho una persona más fuerte. A mi mamá, por apoyarme desde el principio y darme fuerzas para seguir adelante.

Un agradecimiento especial al profesor Javier Madroñero y a William Salazar por su ayuda, paciencia y apoyo. William ha sido como un papá para mí, y le debo mucho de lo que está en este trabajo y de lo que he aprendido.

A mis amigos de cohorte, a mis mejores amigos Steven Sánchez y Camilo Taborda; a mi mejor amiga, Isabel Cristina Mallama, y a su esposo Magnus; y también a toda la familia Pérez.

A mis compañeros José Cuenca, a todos los compañeros de QuanTIC, de mi cohorte, a los compañeros de la clase de alemán, a los profes Hernán Ocampo, Yamit Yalanda y Luz Marina, a quienes participaron en la rifa, y a todas las personas que han sido parte de mi vida en algún momento. Muchas gracias a todos.

1 Introduction

The Bose-Einstein Condensate (BEC) has been of great relevance in the physics of the condensed matter and the quantum statistical mechanics. [1]. It opens new perspectives in various areas such as quantum optics, coherent control, quantum simulation, etc. [2] It was first theorized in 1924 by Bose [3] and Einstein [4] but it wasn't until the year 1994 that the first experiments were carried out by Cornell and Wieman [5], Ketterle [6], and Hulet [7, 8]. It is known that in order to trap and cool down a BEC different kind of traps have been developed, including optical lattices [2, 8], generated by counter-propagating laser beams, as a consequence periodic standing waves are generated whose wavelength is on the order of a few hundred nanometers [9, 10]. The interaction between two BECs has aroused particular interest due to the great variety of phenomena associated with the exchange of particles between the BECs, such as π oscillations, Josephson effects or coherent oscillations [11]. This kind of systems (also known as dimers or Josephson bosonic junctions) consist of many ultracold atoms in double wells. Therefore, the models developed for the description of a cold boson gas in a lattice are adapted to this class of systems. One of the best established models is the Bose-Hubbard [12], whose Hamiltonian includes the interaction of particles in the same well and the hopping of particles between neighboring sites [13] . The Bose-Hubbard model combined with the mean field approximation leads to a semiclassical description of the BEC dimer. It should be noted that dimers with symmetrical wells have been widely studied theoretically [11, 14–16] and experimentally [17, 18]. This project explores the boson system in an asymmetric double well, which can be produced, for example, by a static field or by gravity effects at the mean field limit. The following chapter presents the theoretical background, along with the fundamental concepts relevant to this study. Subsequently, the semiclassical mean-field approximation is examined, followed by an analysis of the same dimer system using the spin formalism. Finally, the findings of the study using both approaches are discussed.

2 Theoretical Background

This chapter briefly introduce the basic fundamental concepts necessary to clearly understand this work. We start with some basic solid state concepts, such as the energy band structure of particles under a periodic potential, then a quick introduction to the Bose-Hubbard model for ultra-cold atoms, and finally we take a look at the Wannier-Stark effect, whose properties are of special interest in this work.

2.1 Energy bands for a one-dimensional periodic potential

We wish to study how a Bose-Einstein Condensate behaves in an optical lattice. The simplest form of such lattice is the result of two counter-propagating laser beams and can be expressed in one dimension as a periodic potential [2, 19] of the form

$$V(x) = V_o \cos\left(\frac{2\pi}{a}x\right) = V_o \cos\left(k_L x\right),$$

where V_o is the intensity of the laser beam and k_L is the propagation vector of the laser beam. First, we consider the Hamiltonian of a single particle H_{one} in one dimension, *i.e* neglecting, by now, the interaction between the particles and external linear force. Such Hamiltonian only has a kinetic energy and the periodic potential mentioned above, so that it reads

$$H_{\text{one}} = \frac{p^2}{2m_o} + V(x), \tag{1}$$

with p and m_o being the particle's momentum and mass, respectively. According to the Bloch's Theorem, the eigenfunctions of H_{one} are given by $\psi_k^\alpha = e^{i\kappa x}u_\kappa^\alpha(x)$, where the Bloch's function $u_\kappa^\alpha(x)$ satisfies the same translational or periodic symmetry as $V(x)$ does, that is $V(x) = V(x+d)$ and $u_\kappa^\alpha(x) = u_\kappa^\alpha(x+d)$. Here κ represents a quasimomentum and α the band index. Replacing the eigenfunctions in (1), we can obtain the time-independent Schrödinger equation

$$\left[\frac{(p+h\kappa)^2}{2m_o} + V(x)\right] u_\kappa^\alpha(x) = E_\kappa^\alpha(x) u_\kappa^\alpha. \tag{2}$$

Moreover, the Bloch's functions can be written as Fourier series as

$$u_\kappa^\alpha(x) = \sum_n u_n(\alpha,\kappa) e^{i2\pi n\frac{x}{a}}. \tag{3}$$

Replacing (3) in (2), we obtain:

$$\left[(k+n)^2 + \int_{-a}^{a} e^{i2\pi(n-m)\frac{x}{a}}\frac{V(x)}{E_r}dx\right] u_\kappa^\alpha(\alpha,k) = \epsilon_k^\alpha u_\kappa^\alpha(\alpha,k),$$

where $k_L = 2\pi/a$, $E_r = \hbar^2 k_L^2/2m_o$, $k = \kappa/k_L$ is dimensionless quasimomentum and $\epsilon_k^\alpha = E_\kappa^\alpha/E_r$ is dimensionless energy. Replacing the periodic potential $V(x)$ mentioned earlier, the matrix elements of the matrix we want to diagonalize are given by

$$\left[(k+n)^2\delta_{n,m} + \frac{V_o}{E_r}a(\delta_{n,m+1} + \delta_{n,m-1})\right] u_\kappa^\alpha(\alpha,k). \tag{4}$$

We can obtain numerically an expression for $\epsilon_k^\alpha(k)$. Setting $E_r = k_L = a = 1$ and $n = m = 5$, *i.e.* a 5×5 matrix, the eigenvalues plotted in Mathematica[1] are shown in Figure 1. We can see that the energy bands do not cross with each other, unlike if we have terms with $\delta_{n,m+s}$, with $s \neq 1$. The functions' energy gap and "smoothness" increase with the potential V_o.

[1] It is important to note that all the remaining results in this work were obtained using Mathematica and Python.

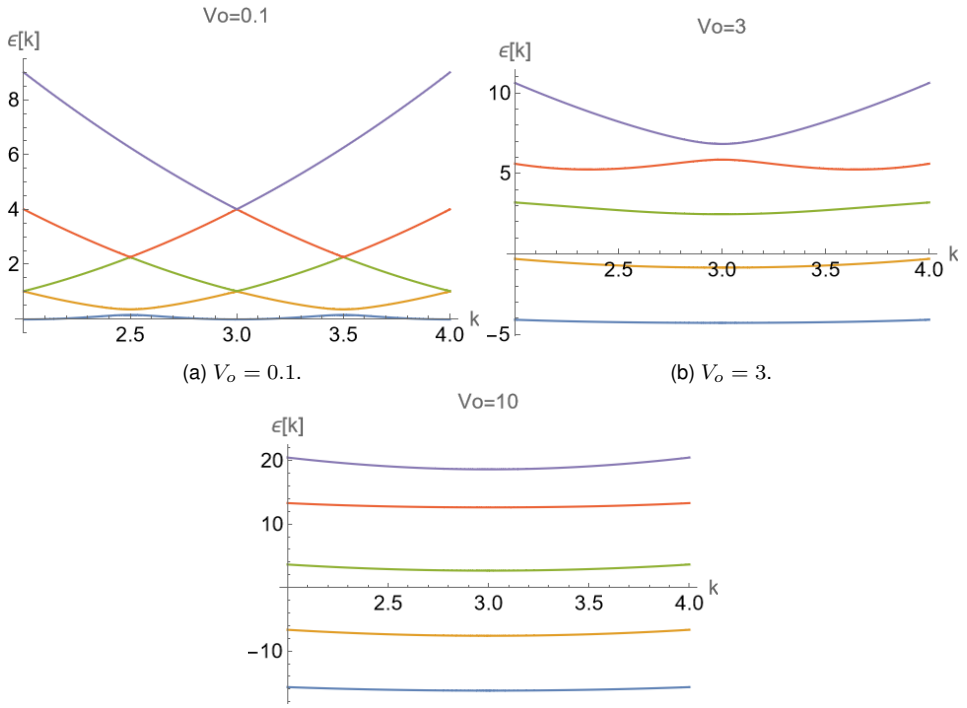

(a) $V_o = 0.1$.

(b) $V_o = 3$.

(c) $V_o = 10$.

Figure 1: Eigenenergies $\epsilon_k^\alpha(k)$ in terms of the dimensionless quasimomentum k varying the values of V_o.

2.2 Bose-Hubbard Model for ultracold atoms

The Bose-Hubbard model is a versatile tool for modeling several systems in the condensed matter and quantum systems, such as ultracold atoms, localization phenomena, quantum phase transitions, quantum computations and quantum information processing, among others. [24–26]

Historically, it was first proposed the Hubbard model, which studies the behavior of a gas of valence electrons under a periodic potential (lattice of the atoms). Later there was introduced the Bose-Hubbard model to study bosons under the same periodic potential [30]. It was realized that one can use this model on ultracold atoms in optical lattices by replacing the electrons with bosons which would act as ultracold atoms. Because of its high degree of controllability and precision, studying ultracold atoms in optical lattices is more advantageous than solid state systems. Moreover, the interactions can be controlled via Feschbach resonances [2]. The Bose-Hubbard model is described by the following Hamiltonian [25],

$$\hat{H}_{\text{BHM}} = -J \sum_{\langle i,j \rangle} \left(\hat{a}_i^\dagger \hat{a}_j + \hat{a}_j^\dagger \hat{a}_i \right) + \sum_i \frac{U}{2} \hat{n}_i (\hat{n}_i - 1) + \mu \sum_i \hat{n}_i, \tag{5}$$

where $\hat{a}^\dagger$, $\hat{a}$ and $\hat{n}$ are the boson creation, annihilation and number operators of particles, respectively. The symbol $\langle ... \rangle$ represents here that the sum is restricted only to nearest neighbors over the whole lattice. J and U are experimental parameters and μ is the chemical potential. The first term, with the parameter J, is the tunneling or hopping term where we can see the term $\hat{a}_i^\dagger \hat{a}_j$ as the movement of a boson from one site to the other, or said formally the destruction of the boson at the j-th site and the creation of a boson at the i-th site, and the same with the other term. The second term represents the interaction potential among bosons (two or more) within the same site.

Note that if we have only one atom in one site ($\hat{n}_i = 1$), this term would vanish. The third term stands for the chemical potential times the total number of particles.

There are two main regimes at 0 K temperature within the thermodynamic limit: the superfluid and the Mott insulator regime. Depending on the ratio of $\frac{J}{U}$, the system can either be in one of those [27]. The superfluid regime occurs when the tunneling parameter J dominates over the interaction strength U, *i.e.* when $J/U \gg 1$. In this regime, the bosons are not localized across the lattice due to the strong tunneling between sites. Since the particles are not confined to individual wells, the system behaves like a big quantum state with long-range phase coherence. As a consequence, the ground state of the system, the so-called "infinitely shallow lattice" (unlike "infinitely deep lattice" as in the Mott regime) [28], can be described as a superposition of bosons covering the whole lattice and the particles occupy the same quantum state, such as a Bose-Einstein Condensate. In this regime, the energy fluctuations are minimized and the variance of the number of particles operator per site is close to zero ($\hat{\sigma}_i = \left(\langle \hat{n}_i^2 \rangle - \langle \hat{n}_i \rangle^2\right)^{1/2} \approx 0$) [27]. Moreover, the phase diagram exhibits an excitation spectrum with no gaps. The system in this regime is highly sensitive to external perturbations such as changes in the chemical potential or the lattice depth [27].

On the other hand, the Mott insulator regime occurs when the on-site interaction strength U dominates over the tunneling or hopping amplitude J, *i.e.* when $J/U \ll 1$. In this regime, the repulsive interactions between bosons are so strong that they prevent multiple particles from occupying the same lattice site, leading to the localization of particles at individual wells, leading to the system losing phase coherence [27]. Here the variance of the number of particles operator per site is non zero ($\hat{\sigma}_i = \left(\langle \hat{n}_i^2 \rangle - \langle \hat{n}_i \rangle^2\right)^{1/2} > 0$) and the system is characterized by an energy gap between the ground state and the first excited state, because adding or removing a boson in each site requires energy and such energy is proportional to the interaction strength U, or in other words, the stronger the interactions between particles, the more energy is required to add or remove a particle, leading to a larger energy gap [24, 27]. Because of the fixed number of particles per site, the Mott insulator is said to be incompressible and small changes in the chemical potential μ won't vary the distribution of bosons at each site nor any small external perturbations. Unlike the superfluid phase, its phase diagram is shown as an excitation spectrum with gaps, and each site is effectively decoupled from its neighbors [27].

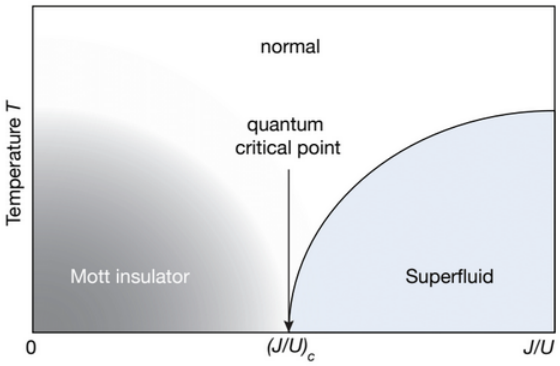

Figure 2: Sketch of the phase diagram of the Bose-Hubbard model, showing the temperature T as a function of the ratio $\frac{J}{U}$. Here the two quantum phases, Mott insulator and superfluid are observed. When $T \gg 0$, the "normal" phase emerges, where the quantum properties of the gas are lost, and the bosons behave as a classical Bose gas. Taken from [29, 32].

Moreover, the transition between the superfluid and Mott insulator phases is a quantum phase

transition that occurs at zero temperature due to quantum fluctuations. As mentioned above, the critical point of the transition is determined by the ratio J/U, more specifically a critical value $(\frac{J}{U})_c$. This ratio is tuned by adjusting the parameters J and U (for instance, through changes in the lattice depth or via Feshbach resonances). In an optical lattice, this phase transition has been experimentally observed in cold atom systems, where ultracold bosonic atoms are trapped in periodic potentials formed by interfering counter-propagated laser beams [2, 27]. By varying the lattice depth, the tunneling or hopping amplitude J can be finely controlled, allowing precise system tuning across the superfluid-Mott insulator transition. Additionally, the parameter U can be tuned using Feshbach resonances: By applying an external magnetic field, one can modify the interaction strength between two scattering particles, which is proportional to U. These experiments have confirmed the theoretical predictions of the Bose-Hubbard model and highlighted the importance of quantum correlations and interactions in driving the phase transition [27].

The experimental realization of the Bose-Hubbard model using ultracold atoms in optical lattices has provided a direct observation of the superfluid-to-Mott insulator transition, making it one of the most significant milestones in quantum simulation. Ultracold atoms are an ideal platform for simulating the Bose-Hubbard model because of their high degree of tunability and the ability to control both the interaction strength U and the hopping amplitude J. This experimental control has allowed researchers to explore the phase diagram of the system, including both equilibrium and non-equilibrium dynamics of the superfluid and Mott insulating phases [2]. Moreover, understanding the superfluid and Mott insulator regimes has several implications in other areas of physics, such as quantum information processing and condensed matter physics: the superfluid regime is also closely related to the behavior of superconductors and superfluids in real materials. In contrast, the Mott insulator regime provides insights into strongly correlated electron systems and the physics of high-temperature superconductors [2, 27].

2.3 Wannier-Stark effect

The Wannier-Stark effect refers to the movement of particles in a lattice subjected to a constant external field. It was originally discovered in the context of solid-state physics, the effect arises when a periodic potential, *e.g.* as an atomic lattice, is combined with a uniform electric field [33, 35–38]. The external field tilts the potential, causing energy levels within the lattice to shift and localize. When a constant external field F is applied, it adds a linear potential to the Hamiltonian

$$\hat{H} = \hat{H}_o + Fx,$$

where $\hat{H}_o$ is the Hamiltonian of the particle in the periodic potential, and Fx is the potential energy due to the external field. The presence of this linear term breaks the translational symmetry of the system, and the energy spectrum changes from continuous energy bands to a Stark ladder of discrete levels [34]. On the other hand, the energy eigenvalues in the presence of the external field are given by

$$E_n = E_o + n\Delta E,$$

where $\Delta E = Fa$ is the energy difference between successive sites and a is the lattice parameter. These quantized levels, known as Wannier-Stark ladders, show the localization of the particle due to the external field F [34]. The Wannier-Stark effect causes the particle to spatially localize around certain lattice sites, which differs to the case of Bloch oscillations, where the particle delocalizes across the lattice without dissipation [39, 40]. The Wannier-Stark effect has been observed in several physical systems, from solid-state crystals to ultracold atoms in optical lattices [34, 41]. In optical lattice experiments, the Wannier-Stark effect is studied through the application of a

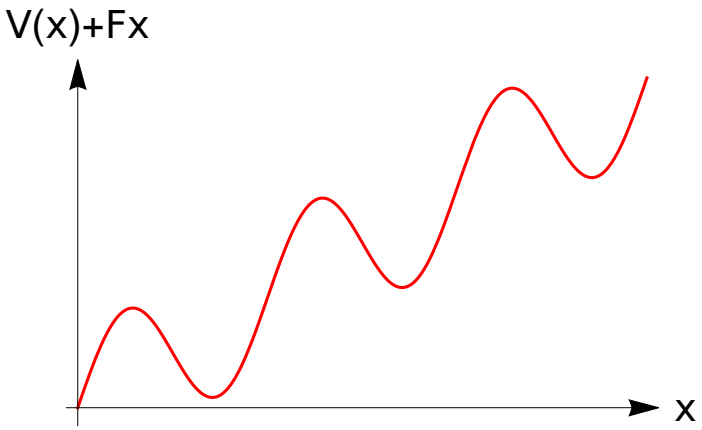

Figure 3: Scheme of the asymmetrical Wannier-Stark potential in one dimension x. Under all the considerations mentioned in the last section, we wish to add an external linear potential $V_{ext} = Fx$, so the double well will be asymmetric.

controlled external field, such as gravity or a magnetic gradient. Such experimental setup has enabled us to directly observe Bloch oscillations, Stark ladders, and Wannier-Stark localization in cold atomic gases [41, 42]. In solid-state physics, the Wannier-Stark effect is useful, particularly in the design of semiconductor superlattices and quantum wells [40, 43]. It also has applications in quantum transport [40] and electron mobility in devices [44] among others, due to its ability to control electron localization through external fields.

3 Semiclassical mean field approximation

In this chapter, we take a look at the interesting case in which we have a large number of ultracold bosons within two optical lattices, also known as dimer[2]. This system is studied semiclassically for two different cases: the isotropic case, meaning that the optical lattice is symmetric therefore the Wannier-Stark effect is absent, and the anisotropic case, meaning that the optical lattice is asymmetric and therefore tilted where the Wannier-Stark effect can be observed. The first case, the symmetry dimer, has already been studied in the literature and it is revised here so that we have a foundation to study the anisotropic dimer, which is new in the literature and also compared to the previous case.

3.1 The isotropic case

Since our purpose is to study the dynamics of a bosonic dimer, we start the description of our system with the Bose-Hubbard model (5). Observe that all the terms of this Hamiltonian run over all sites. However, to explore the dimer case, we restrict the summation to only two sites, yielding

$$H_D = -J(\hat{a}_1^\dagger \hat{a}_2 + \textit{h.c}) + \frac{U}{2}(\hat{n}_1(\hat{n}_1 - 1) + \hat{n}_2(\hat{n}_2 - 1)). \tag{6}$$

Since we study a system with a fixed and significantly large number of particles, we neglect the term involving the chemical potential μ, since in a closed system, it remains constant and merely shifts the energy without affecting the dynamics. We calculate the expected value of the dimer Hamiltonian using coherent states $|\alpha_1\alpha_2\rangle$. Recall that the coherent states of two wells are

$$|\alpha_1\alpha_2\rangle = \sum_{n,m}^{\infty} \frac{\alpha_1^n \alpha_2^m}{\sqrt{n!m!}} e^{-\frac{(|\alpha_1|^2+|\alpha_2|^2)}{2}} |n_1 n_2\rangle, \tag{7}$$

where α are the eigenvalues of the annihilation operator $\hat{a}$. Note that it is an infinite sum, therefore we reach a regime where we work with an infinite number of particles. Thus, coherent states are particularly useful for approximating within such a specific regime.

From the first term of (6) we get

$$\begin{aligned}\langle\alpha_1\alpha_2|\hat{a}_1^\dagger\hat{a}_2 + \textit{h.c}|\alpha_1\alpha_2\rangle &= \alpha_1^*\alpha_2 + \alpha_1\alpha_2^* \\ &= |\alpha_1||\alpha_2|\left(e^{-i(\theta_1-\theta_2)} + e^{i(\theta_1-\theta_2)}\right) \\ &= 2|\alpha_1||\alpha_2|\cos(\theta_1-\theta_2),\end{aligned}$$

with $\alpha_j = |\alpha_j|e^{i\theta_j}$, $j = 1, 2$. Performing a similar calculation, we get the expected value of the second term

$$\langle\alpha_1\alpha_2|(\hat{n}_1(\hat{n}_1 - 1) + \hat{n}_2(\hat{n}_2 - 1))|\alpha_1\alpha_2\rangle = |\alpha_1|^4 + |\alpha_2|^4.$$

Writing together this calculation and considering the difference of the phase of the coherent states $\phi = \Delta\theta = \theta_1 - \theta_2$, the total number of particles $N = |\alpha_1|^2 + |\alpha_2|^2$ and the imbalance or the difference of population between the first and the second well $Z = |\alpha_1|^2 - |\alpha_2|^2$, we obtain

$$\langle H_D\rangle = -J\sqrt{N^2 - Z^2}\cos(\phi) + \frac{U}{4}(Z^2 + N^2).$$

[2]The name *dimer* comes from Biology and Chemistry, and means a structure made of two similar units or monomers, or simply a polymer of two units. Here it is referred to as two identical potential wells or optical lattice sites.

Let's define a new variable $z = Z/N$ and $\mathcal{H} = \langle H_D \rangle / JN$, we obtain

$$\begin{aligned}\mathcal{H} &= -\sqrt{1-z^2}\cos(\phi) + \frac{UN}{4J}(z^2+1) \\ &= -\sqrt{1-z^2}\cos(\phi) + \frac{UN}{4J}z^2 + \frac{UN}{4J}.\end{aligned}$$

Note that the last term in blue represents a shift in the eigenenergies of the system, so we can neglect it. Setting $\Lambda = \frac{UN}{2J}$, we get

$$\mathcal{H} = \frac{\Lambda z^2}{2} - \sqrt{1-z^2}\cos(\phi). \tag{8}$$

ϕ and z are canonically conjugated variables [11, 45], and $[\hat{\phi}, \hat{z}] = i\hbar_{\text{eff}}$, where $\hbar_{\text{eff}} \sim 1/N$ [47]. This turns out to be a semiclassical Hamiltonian if we consider $N \to \infty$, because $\hbar_{\text{eff}} \to 0$. The Hamilton equations of (8) are given by

$$\begin{aligned}\dot{z} &= -\sqrt{1-z^2}\sin(\phi), \\ \dot{\phi} &= \Lambda z + \frac{z\cos(\phi)}{\sqrt{1-z^2}}.\end{aligned}$$

Once the dynamical equations are obtained, we know from Classical Mechanics that the fixed points of these equations represent stable configurations. Thus, the fixed points of this semiclassical Hamiltonian (8) represent quantum stable configurations. We can find the fixed points making $\dot{\phi} = 0$ and $\dot{z} = 0$. Therefore, if $\phi = 0$, then

$$\dot{\phi} = \left(\Lambda + \frac{1}{\sqrt{1-z^2}}\right) z = 0,$$

where we have two possibilities: $z = 0$ and $z_\pm = \pm\frac{(\Lambda^2-1)^{1/2}}{\Lambda}$. If $z = 0$, then

$$\dot{z} = -\sin(\phi) = 0,$$

then $\phi = 0, \pi$. Now, to classify these fixed points: $(z_*, \phi_*) = (0,0), (0,\pi), (\frac{(\Lambda^2-1)^{1/2}}{\Lambda}, 0), (-\frac{(\Lambda^2-1)^{1/2}}{\Lambda}, 0)$, we must obtain the Jacobian matrix evaluated on each of these points and obtaining its eigenvalues. For (0,0):

$$J_{(0,0)} = \begin{pmatrix} 0 & -1 \\ 1+\Lambda & 0 \end{pmatrix} = J_{(0,\pi)},$$

its eigenvalues are $\pm\sqrt{-1-\Lambda}$, so it's an unstable fixed point. Doing a similar process with $J^*_{(\pm\frac{(\Lambda^2-1)^{1/2}}{\Lambda},0)}$, we get the eigenvalues

$$\pm\frac{\sqrt{-\sqrt{\frac{1}{\Lambda^2}}-\Lambda}}{\sqrt{\frac{1}{\Lambda^2}}\sqrt{\Lambda}},$$

therefore, it's an unstable fixed point. Finally, we can obtain the phase space of (8). Note that there is a bifurcation point between $0.5 \leq \Lambda \leq 1.5$. We also can see all the stable fixed points found above. From the Figure 4, we see the interesting behavior of the phase space of our system, and that is its symmetry: given any value of Λ, we obtain a perfectly symmetric image to the axis $z = 0$ and $\phi = 0$.

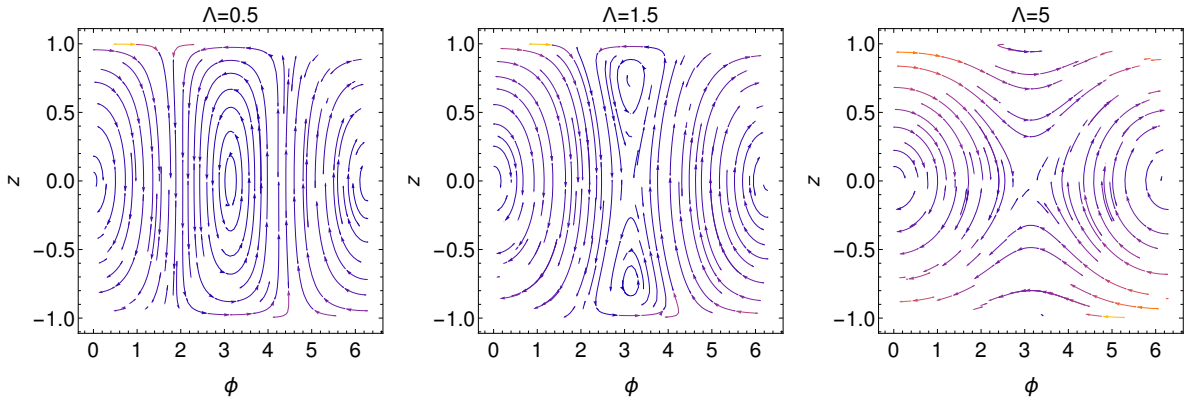

(a) $\Lambda = 0.5$. (b) $\Lambda = 1.5$. (c) $\Lambda = 5$.

Figure 4: Phase space, *i.e.* z vs ϕ, for different values of Λ.

When $\Lambda < 1$ (see Figure 4a), we observe all fixed points are at $z = 0$. This means that one stable configuration of our system occurs when the number of bosons in the first and the second sites are the same (see an example scheme in Figure 5a). As Λ increases, or equivalently $UN > J$, where the interaction effects are much larger than the kinetic ones, the stable fixed points $z_{\pm} = \pm\frac{(\Lambda^2-1)^{1/2}}{\Lambda}$ move further away from each other while remaining equidistant from $z = 0$. This is a direct consequence of their mathematical expressions. Physically, this implies that our system is equally stable when the boson populations in both dimers are equal, *i.e.*, there is no right or left distinction in terms of the system's stability. In Figures 5b and 5c, we can see an exemplification of this property. On the other hand, the stable points at $\phi = (-\pi, 0, \pi)$ do not change with Λ. Recall that these values correspond to the phase differences in the coherent states.

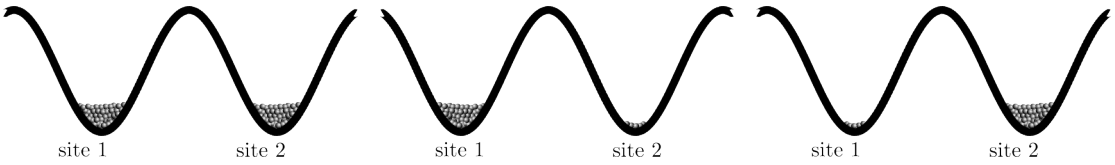

(a) The population of bosons is the same in both sites, i.e. $|\alpha_1|^2 = |\alpha_2|^2$. This case corresponds to the stable fixed point $z = 0$.

(b) We have a given $|\alpha_1|^2 = x$ number of bosons in the first site and a given $|\alpha_2|^2 = y$ number of bosons in the second site.

(c) We have a given $|\alpha_1|^2 = y$ number of bosons in the first site and a given $|\alpha_2|^2 = x$ number of bosons in the second site.

Figure 5: Scheme of three different cases of stable configurations of the isotropic dimer. The second two cases (b) and (c) are indistinguishable in terms of stability.

3.2 The anisotropic case

So far, we have considered the case in which our system is not under the influence of an external potential. In this section, we study our system of interest, which consists of an analogous system with the difference of an external potential V due to an external electric field, for example, whose action on the system results in a tilted potential or tilted periodic lattice, as shown in Figure 3.

Under these considerations, the Bose-Hubbard Model, also called the Wannier-Stark system [35] [36], can be represented as

$$H = -J\sum_{l=1}^{L}\left(\hat{a}_{l+1}^{\dagger}\hat{a}_l + \textit{h.c.}\right) + \frac{U}{2}\sum_{l=1}^{L}\hat{n}_l(\hat{n}_l - 1) + F\sum_{l=1}^{L} l\hat{n}_l + \mu\sum_{l=1}^{L}\hat{n}_l,$$

where L represents the total number of sites of the whole lattice. In this case, we have a term that represents the on-site energy, the sum multiplied by the parameter F, and changes for each site, suggesting that all sites have a different energy that increases one with respect to the previous one. As in the previous case, the last term involves the total number of particles which does not change since we are considering a closed system and thus can be neglected as well. Therefore, the dimer in this case is given by

$$H_{\mathsf{D}} = -J(\hat{a}_1^\dagger \hat{a}_2 + \textit{h.c}) + \frac{U}{2}(\hat{n}_1(\hat{n}_1 - 1) + \hat{n}_2(\hat{n}_2 - 1)) + \epsilon_1 \hat{n_1} + \epsilon_2 \hat{n_2},$$

unlike the isotropic case, we have two additional terms due to the on-site energy variability. Making a calculation analogous to the case of the symmetric dimer, we obtain the semiclassical mean field dynamics in the limit of a large number of particles and restricting the number of wells to two (dimer) is given by the expected value of H_{D} over the coherent states $|\alpha_1\, \alpha_2\rangle$

$$\boxed{\mathcal{H} = \frac{\langle \alpha_1\, \alpha_2 | H_{\mathsf{D}} | \alpha_1\, \alpha_2 \rangle}{JN} = -\sqrt{1 - z^2}\cos(\phi) + \frac{\Lambda}{2} z^2 - \frac{M}{2} z,} \tag{9}$$

where $\phi = \theta_1 - \theta_2$, $z = (|\alpha_1|^2 - |\alpha_2|^2)/N$, $\Lambda = \frac{UN}{2J}$, $N = |\alpha_1|^2 + |\alpha_2|^2$ y $M = \frac{F}{J}$. Note that the variable M contains the symmetry or asymmetry property of the dimer. If $M = 0$, we return to the isotropic case (8). The Hamilton-Jacobi equations are

$$\dot{\phi} = z\Lambda - \frac{M}{2} + \frac{z\cos(\phi)}{\sqrt{1 - z^2}},$$
$$\dot{z} = -\sqrt{1 - z^2}\sin\phi.$$

It is a system of two coupled differential equations whose solution can be found numerically. The phase space of this system is represented in the Figure 7. Unlike the isotropic case, we observe that the only stable points occur when $z \neq 0$. This indicates that the most stable configurations of the system involve a difference in the particle population between the wells. Furthermore, recall that $z = (|\alpha_1|^2 - |\alpha_2|^2)/N$ and in this case $M > 0$, *i.e.* a potential tilted upwards, this implies that there is a tendency for the bosons to be in the first or the second site depending on the difference of phase of the coherent states ϕ. If $\phi = \{0, 2\pi\}$ the bosons will prefer to be in the first site, being in this case the less energetic site. However, if $\phi = \pi$, the bosons will prefer to be in the second site, the most energetic one.

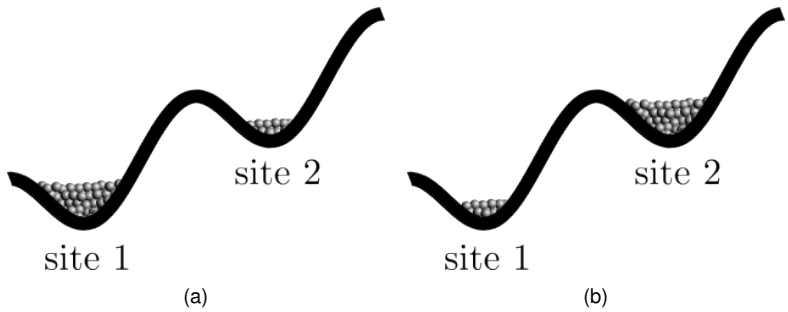

(a) (b)

Figure 6: Under an asymmetric potential well, the bosons preferentially occupy one of the well's sites. We present a schematic representation of two cases: **(a)** where the bosons tend to occupy the less energetic site, and **(b)** where the bosons occupy the more energetic site. In our phase space, case **(a)** corresponds to a phase difference of the coherent states $\phi = \{0, 2\pi\}$, while case **(b)** corresponds to $\phi = \pi$.

Analogously to the case of the symmetric dimer, the fixed point for $z \neq 0$ depends on and increases with the parameter Λ.

The stable points where $\phi = (-\pi, 0, \pi)$ also do not change with Λ and M, which means that the current or movement of particles does not change with these variables. In order to explain this behavior, recall that when we have a Hamiltonian of the form

$$\hat{H}_{\text{example}} = \hat{b}_1^\dagger \hat{b}_2 + \text{h.c.},$$

which describes a particle created at the first site and annihilated at the second site. When computing the expected value of $\hat{H}_{\text{example}}$ using the coherent states α_1 and α_2, as introduced in the semiclassical dimer chapter, we obtain hence $\langle \alpha_1 \alpha_2 | \hat{H}_{\text{example}} | \alpha_1 \alpha_2 \rangle = |\alpha_1||\alpha_2| e^{\mathrm{i}(\theta_2 - \theta_1)} = |\alpha_1||\alpha_2| e^{-\mathrm{i}\phi}$, with $\phi = \theta_1 - \theta_2$. Thus, whenever $e^{\pm \mathrm{i}\phi}$ appears in the expectation values using the coherent states, it indicates particle movement. If the phase is $+\phi$, it corresponds to movement from site 2 to 1, whereas phase $-\phi$ corresponds to movement from site 1 to 2. Therefore, the fact that ϕ remains constant with and without anisotropy tells us that the external field affects solely the distribution of the particles within the well but not the current or the movement of bosons in the dimer.

Another simpler way to come to the same physical interpretation of the meaning of ϕ is to recall the continuity equation in quantum mechanics

$$\frac{\partial}{\partial t} \rho(\vec{r}, t) + \vec{\nabla} \cdot \vec{J}(\vec{r}, t) = 0,$$

where $\rho(\vec{r}, t)$ is the density of probability and $\vec{J}(\vec{r}, t)$ the current of flux of probability for a given wave function $\psi(\vec{r}, t)$. The latter is defined as $\vec{J}(\vec{r}, t) = \frac{-\mathrm{i}\hbar}{2m}(\psi^* \nabla \psi - \psi \nabla \psi^*)$. In the case of the coherent states in one dimension, or $\psi(x) = \alpha(x) = |\alpha(x)| e^{\mathrm{i}\theta(x)}$, the current of probability is proportional to the derivative or the change of θ, or mathematically $J \propto \theta'(x) \approx \theta_2 - \theta_1$, because of the chain rule applied to the exponential function. Therefore, we see one more time that the variations or changes of θ are related to the current or flux.

One curious remark that is worth paying attention to: observe that the phase space of the semiclassical Hamiltonian for $\Lambda = 0.5$ and $M = 0$ is very similar to the phase space of a simple pendulum, taking $\phi = \tilde{\theta}$ and $z = \dot{\tilde{\theta}}$, where the tilde variables correspond to the canonically conjugated variables of the simple pendulum system. Meaning that we have a "harmonic oscillator behavior" where the system tends to have the same number of bosons in both sites, which is the only stable configuration. All the other nearest configurations fall into the fixed points, as the same way as falling into a potential well without escape. And we also have a region after the separatrix, where the dynamics become unstable and we do not have fixed points or closed trajectories in the phase-space. As mentioned previously, what matter from this Figure, is to see that having the same number of bosons in the first and second site is the most stable distribution of bosons within the wells for this choice of parameters Λ and M.

Overall, the symmetry with respect to the axis $z = 0$ disappears when we consider an asymmetrical dimer (see Figure 8). This can be analyzed straightforwardly by examining the variable z in these Hamiltonians. In the symmetric dimer Hamiltonian (8), the difference in the boson population, z, is raised to the power of two in all the terms. In contrast, the asymmetric dimer Hamiltonian (9) treats z differently, with terms that do not necessarily involve z^2. This distinction highlights the differences in how the two systems handle the distribution of particles across the dimer.

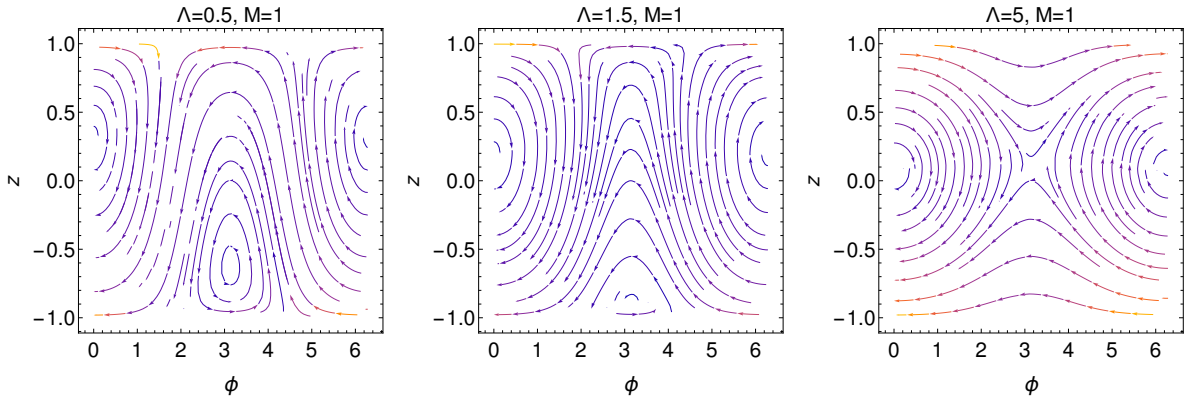

(a) $\Lambda = 0.5$ (b) $\Lambda = 1.5$. (c) $\Lambda = 5$.

Figure 7: Phase space, i.e. z vs ϕ, for different values of Λ and $M = 1$.

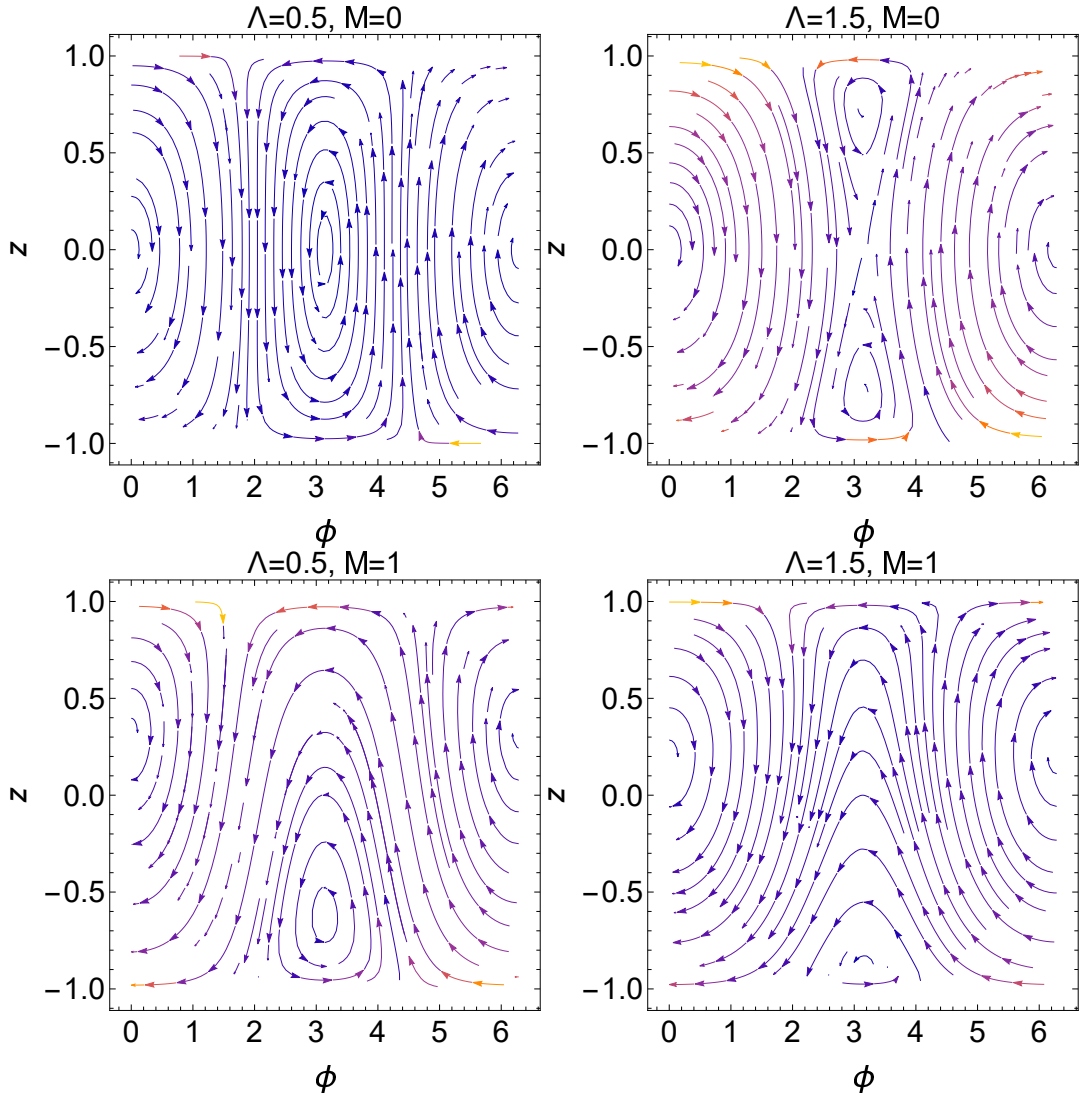

Figure 8: Phase space for different values of Λ and M. The Figures above represent the isotropic case, that is, when the wells are symmetrical, while the Figures below the anisotropic case.

4 Spin representation of the dimer Hamiltonian

Thus far, we have explored the dynamics and stability of both isotropic (symmetric) and anisotropic (asymmetric) dimers within the mean-field approximation. An alternative approach to studying this system is to consider a global spin or a spin dimer representing the collective behavior of all bosons in our optical lattice. Adopting this perspective allows us to explore the implications of anisotropy, understand how the spin components reveal information about the dimer's properties, and identify additional methods for determining the most stable configurations. Furthermore, this approach may provide new insights into the underlying physics and lead to a more comprehensive understanding of the system's behavior.
Let us recall the quantum Hamiltonian for the anisotropic dimer, given by

$$\hat{H}_{\mathsf{D}} = -J(\hat{a}_2^\dagger \hat{a}_1 + \text{h.c.}) + \frac{U}{2}\left(\hat{n}_1(\hat{n}_1 - 1) + \hat{n}_2(\hat{n}_2 - 1)\right) + \epsilon_1 \hat{n}_1 + \epsilon_2 \hat{n}_2.$$

Now since we want to study the behavior near the anisotropic region, let us introduce the following parameters

$$\begin{aligned} w &= \epsilon_1 + \epsilon_2, \\ \Delta &= \epsilon_2 - \epsilon_1, \end{aligned}$$

with $\Delta = 0$ in the symmetrical dimer case and $\Delta \neq 0$ otherwise[3].
We can rewrite the energies per site in terms of these variables as $\epsilon_2 = \frac{w+\Delta}{2}$ and $\epsilon_2 = \frac{w-\Delta}{2}$. Substituting into the Hamiltonian, we get

$$\hat{H}'_{\mathsf{D}} = -J(\hat{a}_2^\dagger \hat{a}_1 + \mathsf{h.c.}) + \frac{U}{2}\left(\hat{n}_1^2 + \hat{n}_2^2\right) + \frac{\Delta}{2}(\hat{n}_2 - \hat{n}_1), \tag{10}$$

where we have neglected the constant term $(\hat{n}_1 + \hat{n}_2)\frac{(w-U)}{2}$. In order to map the dimer Hamiltonian in terms of the spin operators, we introduce a representation of the Bosonic algebra using Schwinger-map [46] given by

$$\begin{aligned} \hat{S}_x &= \frac{1}{2}\left(\hat{a}_2^\dagger \hat{a}_1 + \hat{a}_1^\dagger \hat{a}_2\right), \\ \hat{S}_y &= \frac{1}{2\mathsf{i}}\left(\hat{a}_2^\dagger \hat{a}_1 - \hat{a}_1^\dagger \hat{a}_2\right), \\ \hat{S}_z &= \frac{1}{2}\left(\hat{a}_2^\dagger \hat{a}_2 - \hat{a}_1^\dagger \hat{a}_1\right) = \frac{(\hat{n}_2 - \hat{n}_1)}{2}, \end{aligned}$$

and write down the Hamiltonian H' in terms of these hermitian operators. Notice that these operators satisfy the following commutation relations and reproduce the $SU(2)$ algebra,

$$\begin{aligned} [\hat{S}_x, \hat{S}_y] &= \mathsf{i}\hat{S}_z, \\ [\hat{S}_x, \hat{S}_z] &= -\mathsf{i}\hat{S}_y, \\ [\hat{S}_y, \hat{S}_z] &= \mathsf{i}\hat{S}_x. \end{aligned}$$

So the Hamiltonian in terms of the spin operators turns out to be

$$\boxed{\hat{H}' = -2J\hat{S}_x + \Delta\hat{S}_z + U\hat{S}_z^2 + \frac{UN^2}{4}.} \tag{11}$$

[3] From here we can see the importance of this variable for the subsequent analysis.

This spin dimer Hamiltonian (11) depends only on the $\hat{S}_z$ and $\hat{S}_x$ spin components [4]. The spin in the x-direction $\hat{S}_x$ becomes dominant when we have large values of J, which is the same as being in the superfluid regime. In the Mott insulator regime, and in the case in which we have a large anisotropy, the z-direction component $\hat{S}_z$ becomes dominant.

The term with $\Delta\hat{S}_z$ suggests a Hamiltonian similar to the one in which we have a Zeeman effect produced by an external field in the z-direction. However, this term only appears when $\Delta \neq 0$. This means that the net effect of the anisotropy in our system turns out to be the same as an external magnetic field.

In addition, the spin representation depends on the total number of particles. Recall that $\hat{S}_z = \frac{1}{2}(\hat{n}_2 - \hat{n}_1)$, and the difference of particles in the wells can be $\pm N$, therefore z-spin component $\hat{S}_z$ take values from $-\frac{N}{2}$ to $\frac{N}{2}$, which depends on the total number of particles, and consequently it can take $2\left(\frac{N}{2}\right) + 1 = N + 1$ values. From the spin point of view, the system behaves as a boson, when N is even, and as a fermion when N is odd.

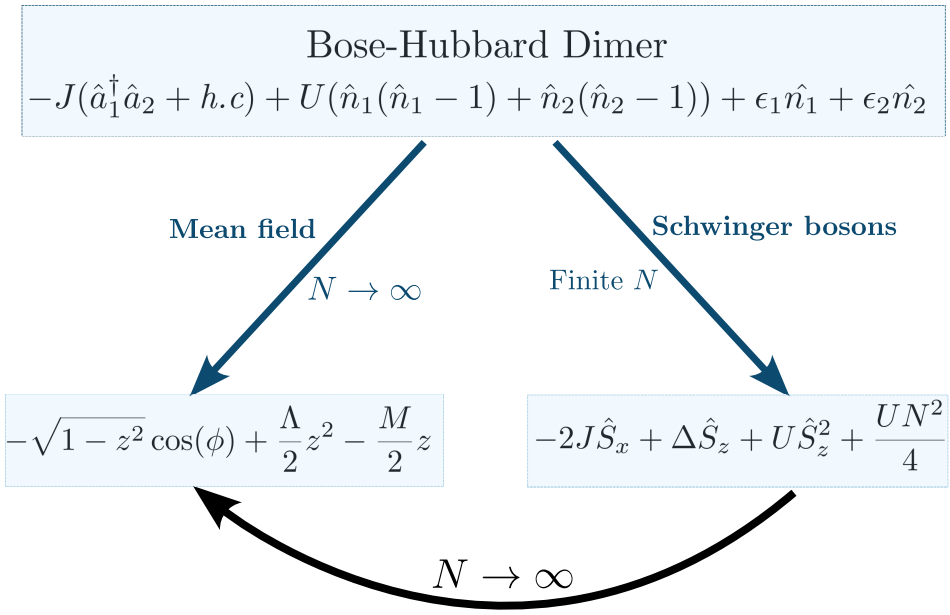

Figure 9: Scheme of the two approaches we use in this work to study the Bose-Hubbard dimer. The first one by using the semiclassical mean field approximation where we have considered a system with a large number of particles, and the second one by using the Schwinger Bosons (spin operations point of view) in which we consider a big net spin of finite N. We can connect both approaches by making $N \to \infty$ from the Schwinger Bosons model.

By completing the square, the previous Hamiltonian (11) can be exactly written as

$$\boxed{\hat{H}' = -J\left(\hat{S}_+ + \hat{S}_-\right) + U\left(\hat{S}_z + \frac{\Delta}{2U}\right)^2 - \frac{\Delta^2}{4U} + \frac{UN^2}{4}.} \tag{12}$$

Notice that if $J = 0$, the minimum of (12) is achieved when the second term is minimized, *i.e.* when the spin in the z-axis $\hat{S}_z = -\frac{\Delta}{2U}$. Again, note that the x-spin component $\hat{S}_x$ is relevant in our Hamiltonian, with a strength controlled by the magnitude of J.

[4] As a special remark, a perturbative treatment of (11) can be done by using the Schieffer-Wolf formalism (see Appendix 5).

4.1 Matrix elements

The dimer spin Hamiltonian shown before can be represented in a matrix form, we just have to calculate $\langle j', m'|H'|j, m\rangle$, where $\{|j, m\rangle\}$ is the set of common eigenstates of $\hat{S}_z$ and $\hat{S}^2$. Recalling the angular momentum theory, we know the result of applying the operators $\hat{S}_\pm$ and $\hat{S}_z$ in this basis $\hat{S}_\pm|j, m\rangle = \hbar\sqrt{j(j+1) - m(m\pm 1)}|j, m\pm 1\rangle$, and $\hat{S}_z|j, m\rangle = \hbar m|j, m\rangle$. Recall that the z-component of the collective spin ranges from $-\frac{N}{2}$ to $\frac{N}{2}$ allowing the Hamiltonian to be represented as a $(N+1)\times(N+1)$ square matrix with matrix elements given by

$$\begin{aligned}\left\langle j', m'\left|\frac{\hat{H}'}{U}\right|j, m\right\rangle = &-\frac{J}{U}\left[\hbar\sqrt{\frac{N}{2}\left(\frac{N}{2}+1\right) - m(m+1)}\delta_{j,j'}\delta_{m,m'+1}\right.\\ &\left.+\hbar\sqrt{\frac{N}{2}\left(\frac{N}{2}+1\right) - m(m-1)}\delta_{j,j'}\delta_{m,m'-1}\right]\\ &+\hbar m\delta_{j,j'}\delta_{m,m'} + \frac{\Delta}{2U}\delta_{j,j'}\delta_{m,m'}\\ &-\left(\frac{\Delta}{2U}\right)^2\delta_{j,j'}\delta_{m,m'} + \frac{N^2}{4}\delta_{j,j'}\delta_{m,m'},\end{aligned} \tag{13}$$

where we have further divided by U to work with dimensionless parameters. Observe that, in this $|j, m\rangle$-basis, (13) is a tridiagonal matrix. The off-diagonal coefficients are given by the term involving the ladder operators, *i.e.* the term with $-\frac{J}{U}$. Note that if $J = 0$, *i.e.* in the Mott insulator regime, we would have a diagonal matrix, meaning also that the energies of the spin system point out in the z-direction and the energies are given by $\tilde{E}_m = \hbar m + \frac{\Delta}{2U} - \left(\frac{\Delta}{2U}\right)^2 + \frac{N^2}{4}$.

However, in general, $J \neq 0$, so it is necessary to diagonalize (13). Since our main interest is to analyze how anisotropy affects the system, we compute and display the eigenvalues over N in Figure 10 as a function of Δ for different values of N. We observe that the first levels are consistently separated from the others, a behavior reminiscent of the band structure in terms of the dimensionless quasimomentum of a particle in a periodic potential (1). However, in this case, we observe a change in the band structure when tuning the number of particles rather than adjusting the external potential.

One of the most intriguing aspects of the energy level structure is the degeneracy occurring when $\Delta/U = 0$ and $\Delta/U \in \mathbb{Z}$. This phenomenon is particularly noticeable in the excited states and becomes more pronounced as N increases. The bands periodically overlap with both preceding and subsequent bands; however, this overlap does not occur with the first band, which corresponds to the ground state.

It is important to recall that this ground state is associated with the z-direction spin, $\hat{S}_z = -\frac{N}{2}$. This indicates that the ground state of the dimer is represented by a negative component of $\hat{S}_z$, pointing downwards. This state will later be used to calculate the expected values of certain operators. Conversely, the degeneracy of the energy bands also arises due to the Zeeman effect discussed earlier in the spin Hamiltonian (11).

If $\Delta/U \neq 0$, a external magnetic field acts on our spin dimer, causing the spectral lines to split or separate, as observed.

The states of the spin dimer Hamiltonian (13) were also obtained. The ground state profile in the $|j, m\rangle$-basis is plotted in the Figure 11. This plot displays the squared components of the ground state vector on the y-axis, with the component indices on the x-axis. Nearly all components are zero,

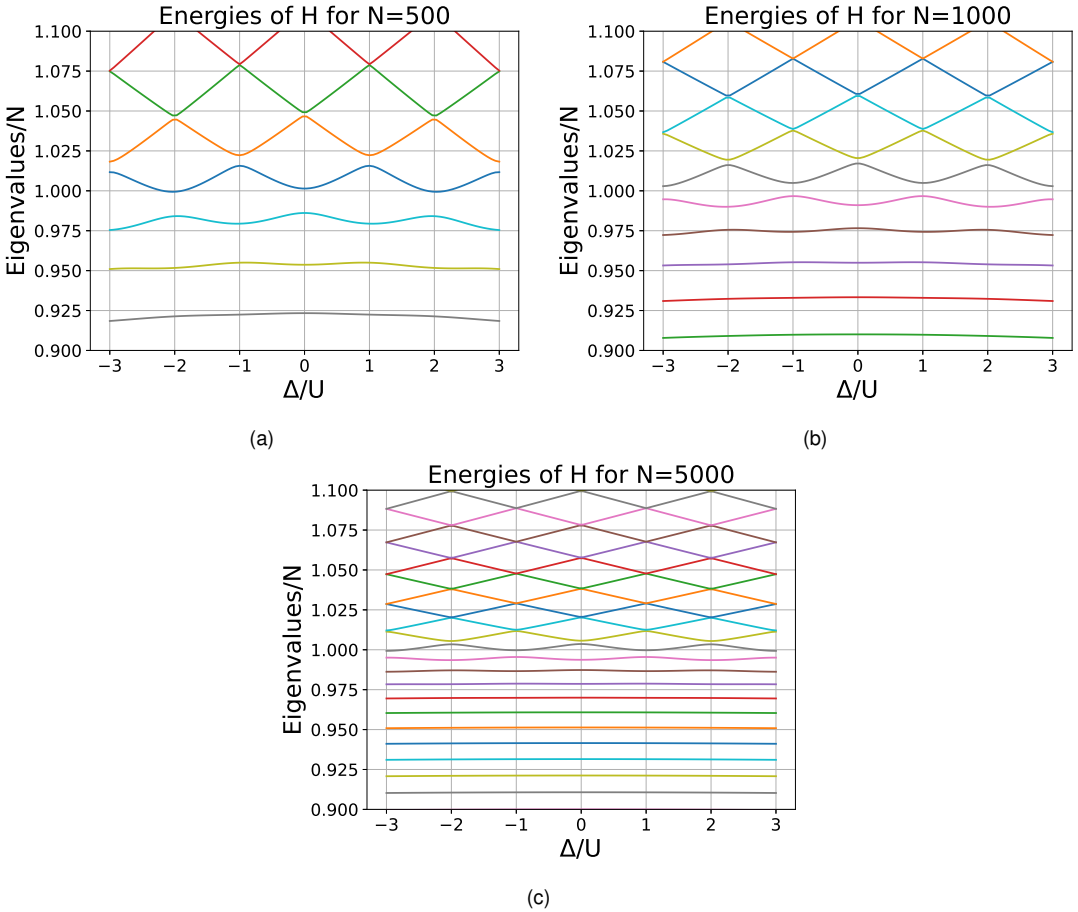

Figure 10: Eigenenergies over N of the spin Hamiltonian matrix representation as a function of Δ for three different numbers of particles N, fixing $\hbar = 1$, $U = 1$, and $J = 1$. It is important to mention that we are only interested in the first energy band, *i.e.* the one corresponding to the ground state. Note that the gap between the first and second energy bands is large and increases as Δ becomes larger, indicating that our system is highly stable in the ground state.

except for a non-zero coefficient near the center, suggesting that the ground state approximates "unitary" vector. Numerically, as we increase the number of particles N, the probability profile increasingly resembles a delta function, indicating that the vector approaches the unit vector $\hat{e}_i$.

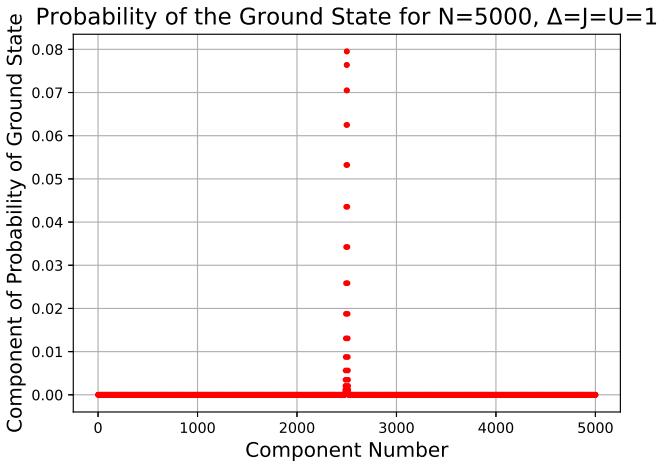

Figure 11: For N=5000 and $\Delta = J = U = 1$, this graph represents the normalized eigenvector values of the ground state vs its components. Note that the majority of its components are zero

.

4.2 Expected values and quantum fluctuations of spin operators

Now, let us proceed to examine the expected values of the spin operators for each component, using the ground state. The expected value, in this context, represents the average outcome we would obtain upon measuring the respective spin operator. This analysis provides insight into the behavior of the quantum system in its lowest energy state, allowing us to predict the likely results of such measurements. $\hat{S}_z$, $\hat{S}_x$ and $\hat{S}_y$ were plotted and shown in Figures 12, 13, and 14, respectively.

In Figure 12a, where the normalized z-direction expected value, $\langle \hat{S}_z \rangle / \left(\frac{N}{2}\right)$, is plotted as a function of $\frac{\Delta}{U}$ and a fixed value of $\frac{J}{U}$ and N, it is observed that the expected value when $\Delta = 0$, that is, when there is no asymmetry in the double well, is null which is to be expected since in the original model the asymmetry is responsible for a net collective spin along the z-axis (see (11)). More specifically, the definition of $\hat{S}_z$ in terms of the Schwinger boson operators is proportional to the difference in population between the two wells, which is zero in the isotropic case.

When $\frac{\Delta}{U} > 0$, *i.e.*, $\epsilon_2 > \epsilon_1$ or an external potential tilted upwards, we observe that $\langle \hat{S}_z \rangle < 0$, indicating that $\hat{n}_1 > \hat{n}_2$. This corroborates the preference of the bosons to occupy the less energetic site under an anisotropic lattice. We can also notice that $\langle \hat{S}_z \rangle$ decreases with $\frac{\Delta}{U}$, until it becomes saturated when $\langle \hat{S}_z \rangle = \frac{N}{2}$, which is the maximum value that this operator can attain and represents the case in which all bosons occupy one site. The analysis is analogous for the $\frac{\Delta}{U} < 0$ case, where bosons tend to occupy the less energetic site, which, in this case, is the second one.

On the other hand, Figure 12b shows how the expected value changes with the experimental parameters of the systems J/U, when Δ/U is fixed and positive. This corresponds to the case of

a tilted upwards lattice. When $J = 0$, the expectation value $\langle \hat{S}_z \rangle$ reaches a minimum at a negative value, suggesting once again that the particles occupy the less energetic well, as $\Delta > 0$.

Additionally, as the hopping term increases, $\langle \hat{S}_z \rangle$ tends toward zero, which aligns with the superfluid regime. In this regime, particle movement between sites is so rapid that an equal number of bosons occupy each site on average, meaning $\hat{n}_1 \approx \hat{n}_2$, and thus $\langle \hat{S}_z \rangle \approx 0$, regardless of the anisotropy value.

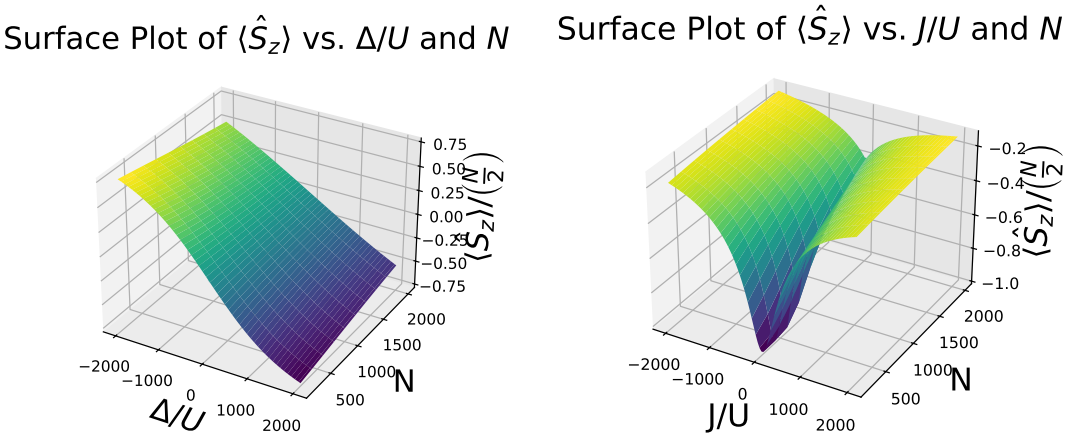

(a) (b)

Figure 12: Normalized expected value of $\hat{S}_z$ varying $\frac{\Delta}{U}$ with $\frac{J}{U} = 800$ (left) and $\frac{J}{U}$ with $\frac{\Delta}{U} = 800$ (right). **(a)** Depending on the asymmetry, notice that when we set the parameter Δ to zero, we essentially remove this source of asymmetry from the system. As a result, the net collective spin along the z-axis vanishes. In other words, when there is no asymmetry in the double well ($\frac{\Delta}{U} = 0$), the quantum system loses its preferential orientation along the z-axis, and this leads to a null expected value. **(b)** There is a maximum at $\frac{J}{U} \gg 1$, suggesting that when the hopping in the system is very large, the component of $\hat{S}_z$ tends to zero as the atoms begin to move between the two wells. This occurs because, when the atoms move so quickly, the populations in each well become nearly equal, making $\hat{S}_z \propto \hat{n}_2 - \hat{n}_1 \approx 0$.

In the same way as with the z axis, the expected values of $\hat{S}_x$ and $\hat{S}_y$ are calculated and presented in the Figures 13 and 14, respectively. We observe that, the expected value $\langle \hat{S}_x \rangle$ has a maximum value $\langle \hat{S}_x \rangle = N/2$ when $\Delta = 0$. In the highly anisotropic case, $|\Delta| \to \infty$, the bosons tend to be in the less energetic well. Therefore, the net spin of the system is entirely a spin pointing in the z-direction causing the x-component to be null. Such behavior is shown in Figure 13a, where $\langle \hat{S}_x \rangle$ decays to zero in both extremes of the plot as Δ increases.

A much simpler explanation can be giving by considering the eigenstates of the $\hat{S}_x$ operator. Let us call them as $|+\rangle = \frac{1}{\sqrt{2}}(|1\rangle + |2\rangle)$ and $|-\rangle = \frac{1}{\sqrt{2}}(|1\rangle - |2\rangle)$, as known from spin-$\frac{1}{2}$ theory, where $|1\rangle$ and $|2\rangle$ represent the sites 1 and 2 of the well, respectively. These $\hat{S}_x$-eigenstates have a null projection in the z-direction. It is straightforward to see that $\hat{S}_x$ has a maximum positive value when the bosons are equally distributed within each site, *i.e.* the isotropic case. Conversely, as the anisotropy increases, causing the bosons to localize in a single site, $\hat{S}_x$ approaches zero.

On the other hand, in the Figure 13b we observe the relationship between $\langle \hat{S}_x \rangle$ and the parameter $\frac{J}{U}$. Here, it is observed that in the superfluid regime, $\langle \hat{S}_x \rangle$ becomes saturated at $N/2$ when $J/U > 0$ and at $-N/2$ when $J/U < 0$. Recall that in such a regime, the particles move very rapidly from one well to the other, so that $\hat{n}_1 \approx \hat{n}_2$. As we discussed above, in such a "quasi-isotropic" case, $\langle \hat{S}_x \rangle$ has a maximum value, whereas $\langle \hat{S}_z \rangle$ is null. It is important to note that the sign change illustrates the movement of particles, *i.e.*, bosons moving from right to left or vice-versa.

Also recall that the $\hat{S}_x$ operator is closely related to the concept of particle flux, as discussed in the third Chapter 3. In contrast, if $\frac{J}{U} \ll 1$ and approaches zero, the particles become more localized in one site since $\Delta \neq 0$. This explains the decay and cancellation around and when it reaches zero, respectively.

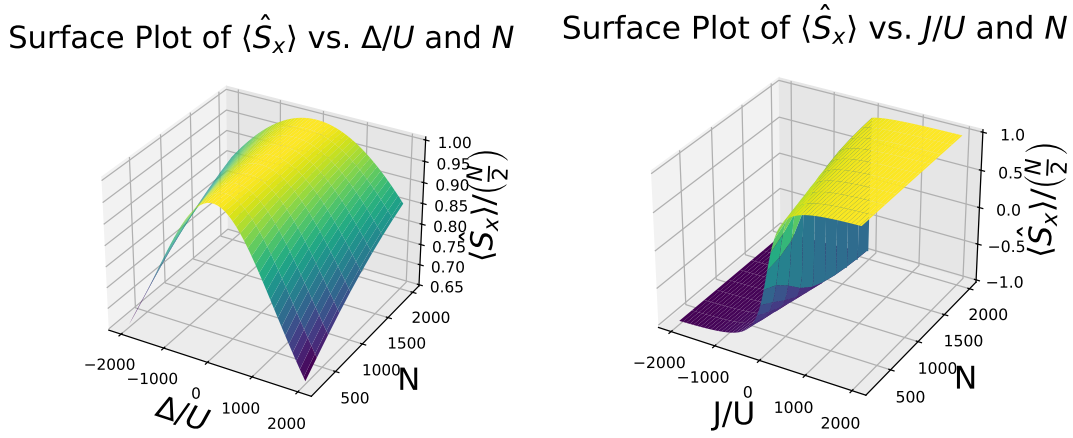

(a) (b)

Figure 13: Normalized expected value of $\langle \hat{S}_x \rangle$ varying $\frac{\Delta}{U}$ with $\frac{J}{U} = 800$ (left) and $\frac{J}{U}$ with $\frac{\Delta}{U} = 800$ (right). **(a)** Dependence on $\frac{\Delta}{U}$. Observe that when the anisotropy Δ is large, the expected value $\langle \hat{S}_x \rangle$ decays to zero. **(b)** In this case, the expected value depends on $\frac{J}{U}$, which saturates for big values of J/U. There is a change in sign with J since this parameter represents the flux or movement from one well to the other.

Figure 14 shows $\hat{S}_y$ plotted as a function of $\frac{\Delta}{U}$ and $\frac{J}{U}$. The figure appears completely empty since its matrix elements are complex. Furthermore, there is no y-spin component in our spin dimer (see (11)).

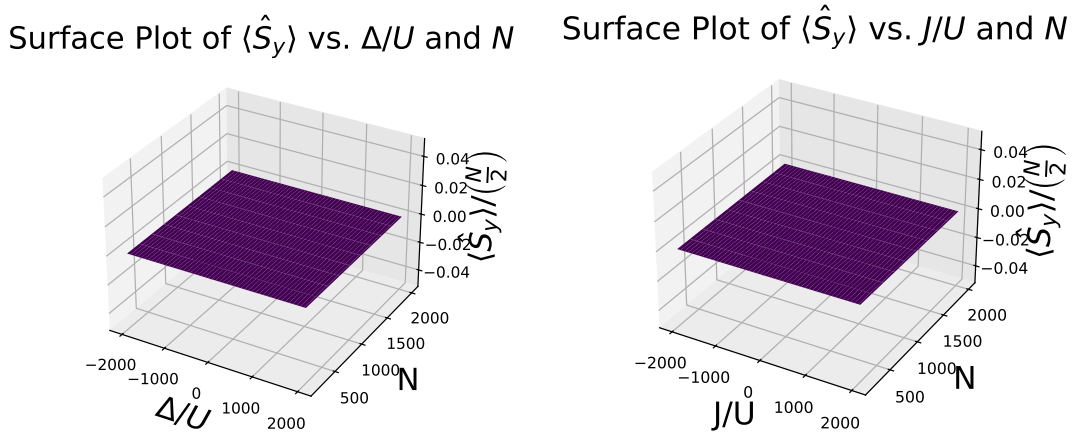

(a) (b)

Figure 14: Normalized expected value of $\langle S_y \rangle$ depending on the parameters $\frac{\Delta}{U}$ and $\frac{J}{U}$.

In addition to the expected values of the spin operators, we can also calculate the spin fluctuations along each axis, defined as

$$\sigma_i^2 = \langle S_i^2 \rangle - \langle S_i \rangle^2, \tag{14}$$

with $i = \{x, y, z\}$. This provides insight into how localized the spin components are along different axes. In this case, we can focus on the fluctuations of $\hat{\sigma}_x$ and $\hat{\sigma}_z$.

Line	Slope	Intercept
$\log(\hat{\sigma}_x^2)$	-1.0259	-1.5721
$\log(\hat{\sigma}_y^2)$	-0.9948	-0.0076
$\log(\hat{\sigma}_z^2)$	-1.0003	-0.2225

Table 1: Average slope and intercept of the lines $\log(\hat{\sigma}_i^2) = \log(\text{const}) - \log(N)$ for $i = \{x, y, z\}$. It is straightforward to see that $\hat{\sigma}_x^2$, $\hat{\sigma}_y^2$, and $\hat{\sigma}_z^2$ decay as $1/N$.

Figure 15a illustrates the dependence of these fluctuations on the parameter Δ/U. The fluctuations in the z-spin component reach their maximum at $\Delta = 0$, indicating minimal localization. This observation is consistent with the isotropic case, where $\langle \hat{S}_z \rangle = 0$ and the net spin aligns entirely along the x-direction. Consequently, fluctuations in the x-direction are minimal, suggesting greater localization along this axis compared to the z-direction.

For larger values of Δ, the situation reverses: bosons tend to localize more strongly in one well, leading to a larger and more defined $\hat{S}_z$ while making $\hat{\sigma}_z$ smaller. Conversely, $\hat{S}_x$ remains small due to the absence of a significant x-component in the dimer spin, causing larger fluctuations in $\hat{\sigma}_x$.

Further insight can be gained by examining how the ration J/U affects quantum fluctuations, as shown in Figure 15b. Fixing a positive Δ/U, we observe that $\hat{\sigma}_z$ reaches its minimum at $J = 0$, which aligns with expectations for the anisotropic case where the bosons remain motionless within the dimer, localizing the spin in the z-direction. At this point, $\hat{\sigma}_x$ reaches a maximum. As J/U increases, both $\hat{\sigma}_z$ and $\hat{\sigma}_x$ evolve, eventually leading to a superfluid regime where particles transition rapidly between wells. In this regime, the net spin predominantly points in the x-direction, and the z-component becomes negligible, causing $\hat{\sigma}_z$ to increase and $\hat{\sigma}_x$ to decrease.

Extending this analysis, we investigate the effect of varying the number of particles N while keeping parameters fixed (Figure 15c). The fluctuations $\hat{\sigma}_x$, $\hat{\sigma}_y$, and $\hat{\sigma}_z$ all exhibit a decay proportional to $1/N$, indicating increasing localization in the semiclassical limit. This behavior is consistent with the theoretical expectation of a $1/N$ decay in many-body systems [47]. To confirm this trend, we replot these quantities on a logarithmic scale in Figure 15d, where straight lines are observed.

Given that $\sigma_i^2 \sim 1/N$, interpreting $\log(\hat{\sigma}_i^2)$ as a function of $\log(N)$ leads to a linear relation where the intercept corresponds to $\log(\text{const})$ and the slope is expected to be -1. The average slopes and intercepts of these logarithmic lines are summarized in Table 1, showing that $\hat{\sigma}_x^2$, $\hat{\sigma}_y^2$, and $\hat{\sigma}_z^2$ all decay as $1/N$.

4.3 Comparison with the semiclassical dimer case

So far, we have explored the dimer using the spin formalism. It is still possible to obtain even more information about our system. The next step is to determine the stability points as we did in the previous chapter, but this time, we approach it from the spin point of view. To do so, we first rewrite our spin Hamiltonian in terms of the parameters Λ and N, as we did for the semiclassical Hamiltonian (9) in Chapter 3, and we express the $\hat{S}_x$ and $\hat{S}_z$ operators as spherical coordinates, i.e.

$$\tilde{S}_x = \frac{\hat{S}_x}{N} = \sin(\theta)\cos(\phi), \tilde{S}_y = \frac{\hat{S}_y}{N} = \sin(\theta)\sin(\phi) \quad \text{and} \quad \tilde{S}_z = \frac{\hat{S}_z}{N} = \cos(\theta).$$

In such a way, we obtain the representation or surface of the Hamiltonian where the points closest to the center or minimum represent values energy minima, and therefore, fixed points of the system.

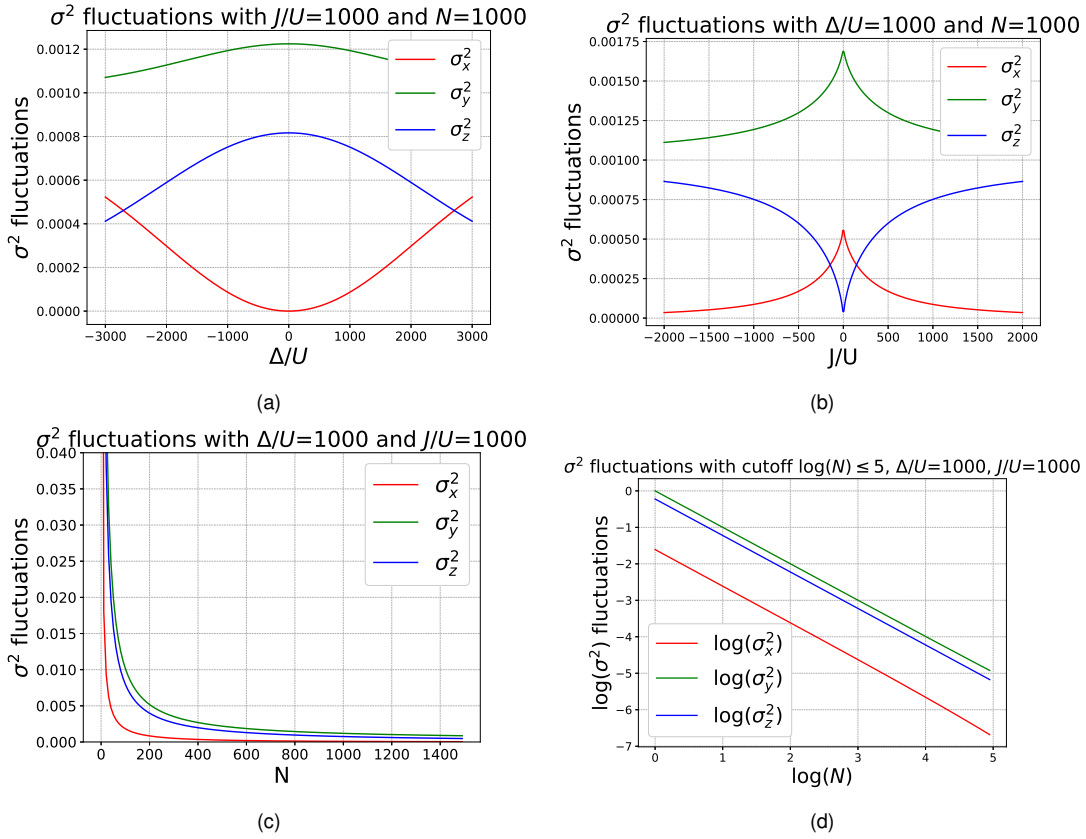

Figure 15: Spin fluctuations depending on $\frac{\Delta}{U}$, $\frac{J}{U}$ and N.

The resulting Hamiltonian is given by

$$\boxed{\tilde{H} = \frac{H}{UN^2} = -\frac{\tilde{S}_x}{\Lambda} + \tilde{S}_z^2 + \frac{\Delta}{UN}\tilde{S}_z + \frac{1}{4},} \quad \text{where} \quad \Lambda = \frac{UN}{2J}.$$

In Figure 16 the Hamiltonian $\tilde{H}$ was plotted in spherical coordinates for $\Lambda = 1$ and 3 different values of Δ. Likewise, in Figure 17 we have a two-dimensional representation of these figures. There, we have plotted the variable ϕ vs θ, and the color represents the value of the Hamiltonian $\tilde{H}$ fixing the value $\Lambda = 1.5$ and varying the parameter Δ.

In Figure 17a , due to the chosen parameters, we consider a symmetric lattice. We can see that the depression is located at $\theta = \frac{\pi}{2}$ and $\phi = \{0, 2\pi\}$, that can be seen as a kidney-shaped surface in Figure 16a with two maxima at the poles and a minimum or mid-level depression. Notice that the surface is symmetric with respect to the $\theta = \frac{\pi}{2}$ and $\phi = \pi$ axes, a property that only occurs when the lattice is symmetric ($\Delta = 0$).

As we increase the anisotropy of our lattice, the minimum point shifts to the right if $\Lambda > 0$ or to the left if $\Lambda < 0$, as shown when $\Lambda = \pm 1$ in Figures 17b and 17c.

This depression or minimum point represents, as mentioned above, a stability point for our system and depends directly on the experimental parameter $\Lambda = \frac{UN}{2J}$, which is called the semiclassical parameter.

Note the strong resemblance between these plots and those obtained in the phase space of the semiclassical Hamiltonian (4). Both results suggest that the system and its stability can be controlled by adjusting the experimental parameters U and J, as well as the asymmetry measure Δ in the spin representation or z in the semiclassical Hamiltonian. In both cases, these variables ultimately correspond to the same physical quantity.

The analysis reveals that, whether in the spin dimer Hamiltonian and the semiclassical one, the isotropic dimer maintains a symmetry or balance in the number of particles occupying each site.

By modifying the parameter Δ of the spin dimer Hamiltonian, we are changing the $\hat{S}_z$ component, which is by definition half the difference of population between the wells. Hence, our spin system is sensitive or conditioned by the asymmetry of the dimer.

By altering Δ, we modify the minimum point of our Hamiltonian surface $\tilde{H}$ along the z axis or the $\hat{\tilde{S}}_z$. As a consequence it moves to the left or to the right by varying Δ without changing its depth or any other component in the other directions $\hat{\tilde{S}}_x$ or $\hat{\tilde{S}}_y$.

Similarly, by adjusting the anisotropy M in the semiclassical case, the fixed point varies only along the vertical direction given by $z = \frac{|\alpha_1|^2 - |\alpha_2|^2}{N}$, while its horizontal component, ϕ, remains unchanged.

4.4 Dimer entanglement

It is possible to explore even more our Bose-Hubbard dimer by analyzing its entanglement properties. A straightforward approach is to study the behavior of the sum of the expected values of x and y and check the inequality

$$\sigma_x^2 + \sigma_y^2 \geq \frac{N}{2},$$

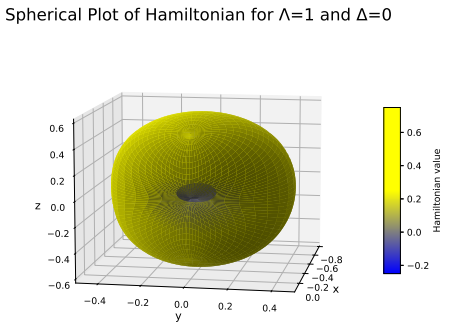

(a) $\Lambda = 1$ and $\Delta = 0$, or symmetrical dimer case.

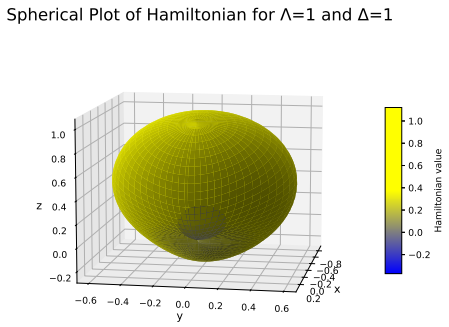

(b) $\Lambda = 1$ and $\Delta = 1$, or tilted upwards lattice case.

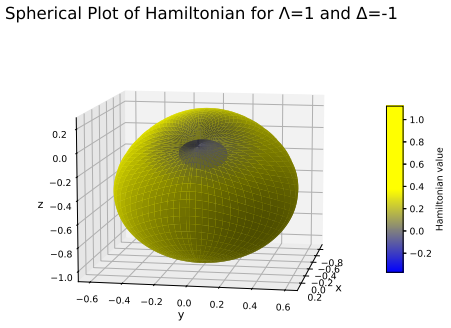

(c) $\Lambda = 1$ and $\Delta = -1$, or tilted downwards lattice case.

Figure 16: Hamiltonian surface or "sphere" $\tilde{H}$ where the spin operators are used as spherical coordinates, and all the other parameters are set to 1.

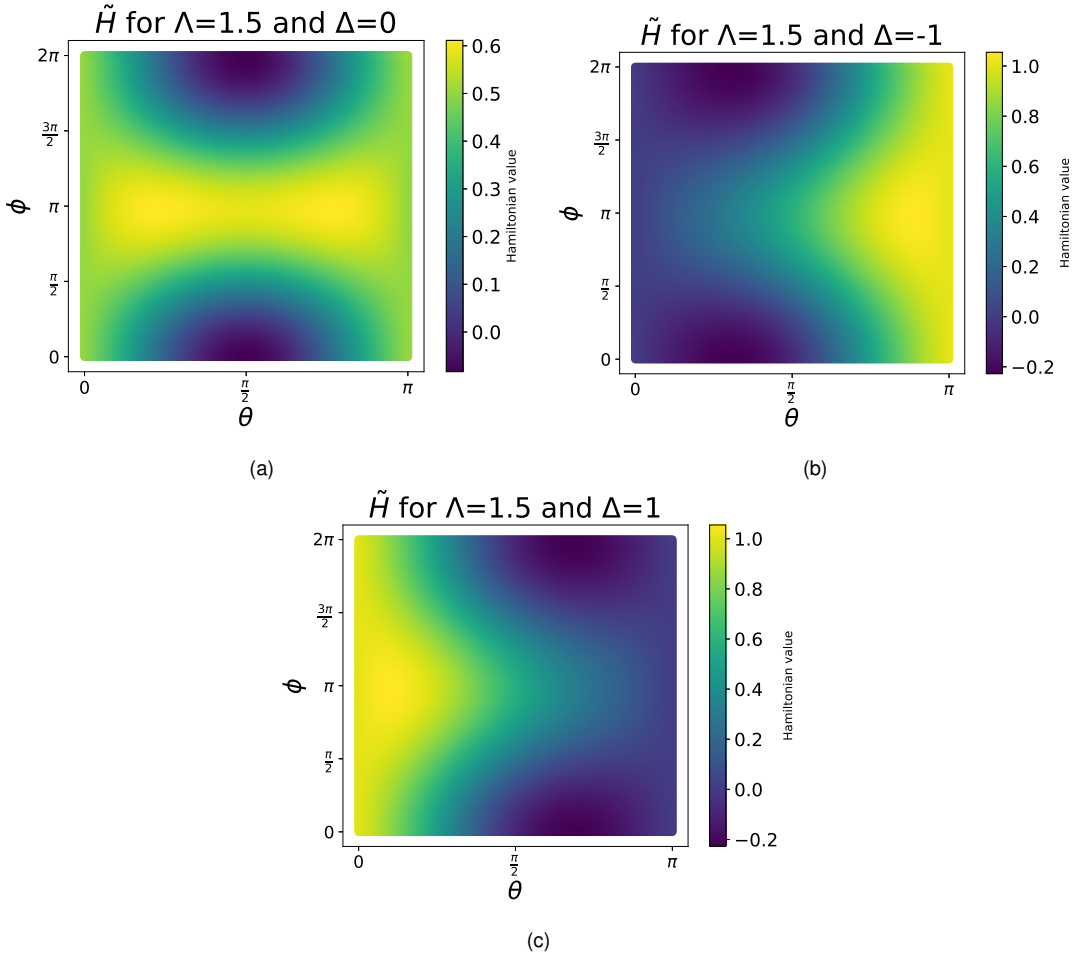

Figure 17: Hamiltonian $\tilde{H}$ as a function of θ and ϕ for $\Lambda = 1.5$ with varying Δ. The blue regions represent the minimum values of the Hamiltonian. In **(a)** the system exhibits symmetry with respect to $\theta = \frac{\pi}{2}$ and $\phi = \pi$ axes. For a tilted lattice, such symmetry disappears as shown in **(b)** and **(c)**. This behavior mirrors that observed in the phase space of the semiclassical Hamiltonian (see (4) in the previous chapter) reinforcing that Δ (in the spin-formalism) and z (in the semiclassical Hamiltonian) correspond to the same physical quantity.

which holds if the system is separable [48]. Unlike previous cases, we now compute the expected values using all the eigenstates of the system, rather than just the ground state. This allows us to determine whether the spin dimer is separable or entangled for both ground and excited states. For clarity, Figure 18 shows the sum of fluctuations for each state. The first state (the 0th) is always entangled, as its sum is consistently below $N/2$.

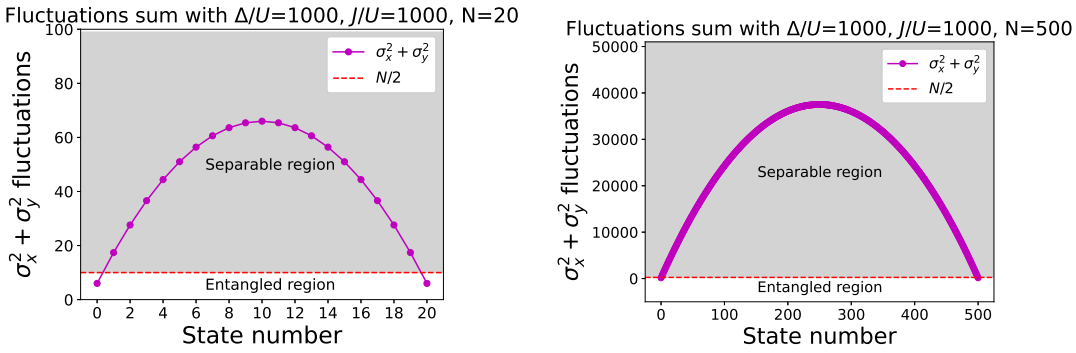

(a) (b)

Figure 18: The sum of fluctuations $\sigma_x^2 + \sigma_y^2$ as a function of the states with fixed parameters for two values of N. The separable region corresponds to values above $N/2$, while the entangled region lies below $N/2$. The ground state remains entangled regardless of the value of N.

5 Conclusions and perspectives

In this work, we investigated the dynamics of a gas of ultracold bosons in a one-dimensional anisotropic or asymmetric two-site optical lattice (*i.e*, a dimer) from two different perspectives. The first approach utilized the mean-field approximation, while the second employed the spin formalism, considering a large number of bosons for both approaches. Our findings revealed that introducing anisotropy through an external field significantly influences the system in various ways. The most notable effect is the symmetry breaking in phase space, which alters the system's stability and fixed points. This phenomenon can be interpreted as a "dissipative" process in the semiclassical dynamics since a term proportional to the momentum emerges, where the population difference z is no longer null at the fixed points. As a consequence, the bosons exhibit a preference for occupying the lower-energy site. However, the overall particle flux remains conserved in both isotropic and anisotropic cases.

From another perspective, the variable z can be understood as a momentum variable. When anisotropy is introduced, a linear term involving z emerges, which can be associated with a dissipative term. In our system, inverting $z \to -z$ corresponds to reversing the direction of time. Consequently, a symmetric dimer is time-reversal invariant.

Examining the system through spin formalism, we found a Zeeman effect, where the dimer behaves as an $N/2$-spin model subjected to an external magnetic field proportional to Δ. This interaction appears in the Hamiltonian as the term $\Delta\hat{S}_z$, which only exists for $\Delta \neq 0$, signifying an asymmetrical potential well. The analysis of the spin dimer Hamiltonian spectrum shows that for $\Delta = 0$, the spectral lines exhibit degeneracy. However, when $\Delta \neq 0$, the degeneracy is lifted, akin to the Zeeman effect.

Furthermore, the z-spin component, $\hat{S}_z$, strongly depends on anisotropy. Since $\hat{S}_z$ represents half the difference in particle numbers between the two sites, modifying the dimer symmetry affects $\hat{S}_z$, reinforcing the tendency of bosons to occupy the lower-energy site in the presence of anisotropy.

One of the key observations concerns the quantum fluctuations of the $\hat{S}_z$ component. As the number of particles increases, the quantum fluctuations $\hat{\sigma}_x$, $\hat{\sigma}_y$, and $\hat{\sigma}_z$ decrease, specifically following $\hat{\sigma}_z \propto 1/N$. This suggests that $\hat{S}_x$, $\hat{S}_y$, and $\hat{S}_z$ become increasingly well-defined in the semiclassical limit, where fluctuations in $\hat{\sigma}_z$ can be neglected.

From a broader perspective, a promising direction for future research is the study of the spin coherent states in this system. These states maximize coherence in spin orientation, thereby minimizing uncertainty in spin direction. This approach provides insights into quantum spin properties and how anisotropy affects coherence and quantum fluctuations. Additionally, within the spin coherent state description, we can explore the threshold for transitioning from a quantum system to a classical one.

Another intriguing direction involves analyzing the system's dynamic response to uncover mechanisms for controlling spin states. Such insights could have implications for quantum information processing and non-equilibrium quantum systems.

Lastly, an alternative perspective is to treat the systems as a qubit or a two-level system, utilizing the ground state for quantum computation and information storage. Encoding information in the ground state allows for leveraging the system's inherent quantum properties for qubit operations. Furthermore, studying the coupling between qubit states and an external field could lead to precise

control mechanisms for qubit manipulation. This perspective not only enhances our fundamental understanding of quantum two-level systems but also holds practical significance for the design of quantum devices and logic gates.

Appendices

A Schieffer-Wolf transformation

To obtain the effective low energy dynamics, we can use the Schieffer-Wolf transformations [49] to solve the spin dimer Hamiltonian (11). First, we will start with a perturbation approach separating such Hamiltonian into two subhamiltonians as

$$\begin{aligned}\hat{H}' &= -2J\hat{S}_x + \Delta\hat{S}_z + U\hat{S}_z^2 + \frac{UN^2}{4}, \\ &= \underbrace{-J\left(\hat{S}_+ + \hat{S}_-\right)}_{V} + \underbrace{\Delta\hat{S}_z + U\hat{S}_z^2 + \frac{UN^2}{4}}_{\hat{H}_o},\end{aligned}$$

where V is a perturbation of $\hat{H}_o$.

Now we will define an effective Hamiltonian $\hat{H}_{\text{eff}} = e^S \hat{H} e^{-S}$, where S represents some unitary matrix.

Expanding $\hat{H}_{\text{eff}}$

$$\begin{aligned}\hat{H}_{\text{eff}} &= \hat{H}\left[S,\hat{H}\right] + \frac{1}{2}\left[S,[S,\hat{H}]\right] + \mathcal{O}(S^3), \\ &= \hat{H}_o + V + \left[S,\hat{H}_o + V\right] + \frac{1}{2}\cancelto{0}{\left[S,[S,\hat{H}_o + V]\right]} + \cancelto{0}{\mathcal{O}(S^3)}, \\ &\approx \hat{H}_o + V + \left[S,\hat{H}_o\right] + [S,V]\,,\end{aligned}$$

choosing an S that satisfies

$$V + [S,V] = 0, \tag{15}$$

then,

$$\begin{aligned}\hat{H}_{\text{eff}} &\approx \hat{H}_o + \underbrace{V + \left[S,\hat{H}_o\right]}_{0} + [S,V]\,, \\ &\approx \hat{H}_o + [S,V]\,.\end{aligned}$$

According to (15), we must find an S such that

$$\begin{aligned}V + \left[S,\hat{H}_o\right] &= 0, \\ V &= \left[\hat{H}_o, S\right], \\ -J\left(\hat{S}_+\hat{S}_-\right) &= \left[\hat{H}_o, S\right],.\end{aligned} \tag{16}$$

Now let $|l\rangle = |\frac{N}{2}, l\rangle$ denote the spin $\frac{N}{2}$ $\hat{S}_z$ eigenstates, therefore

$$\langle l|\left[\hat{H}_o, S\right]|m\rangle = (\epsilon_l - \epsilon_m\langle l|S|m\rangle), \tag{17}$$

where ϵ represent the eigenenergies of the $\hat{H}_o$ subhamiltonian, $\epsilon_l = \Delta l + Ul^2 + \frac{UN^2}{4}$. Moreover, recall the matrix elements of the spin ladder operators is given by

$$\langle l|\hat{S}_\pm|m\rangle = \sqrt{\frac{N}{2}\left(\frac{N}{2}+1\right) - m(m\pm 1)}\delta_{l,m\pm 1}. \tag{18}$$

From (16) and using (17) and (18),

$$\begin{aligned} -J\left(\hat{S}_+ + \hat{S}_-\right) &= \left[\hat{H}_o, S\right], \\ -J\langle l|\left(\hat{S}_+ + \hat{S}_-\right)|m\rangle &= \langle l|\left[\hat{H}_o, S\right]|m\rangle, \\ J\langle l|\left(\hat{S}_+ + \hat{S}_-\right)|m\rangle &= (\epsilon_m - \epsilon_l)\langle l|[S]|m\rangle, \end{aligned}$$

$$\frac{J\left(\sqrt{\frac{N}{2}\left(\frac{N}{2}+1\right) - m(m+1)}\delta_{l,m+1} + \sqrt{\frac{N}{2}\left(\frac{N}{2}+1\right) - m(m-1)}\delta_{l,m-1}\right)}{\epsilon_m - \epsilon_l} = \langle l|S|m\rangle,$$

But $\epsilon_m - \epsilon_l = \Delta(m-l) + U(m^2 - l^2)$, therefore we can determine the matrix elements of S

$$\boxed{\frac{J\left(\sqrt{\frac{N}{2}\left(\frac{N}{2}+1\right) - m(m+1)}\delta_{l,m+1} + \sqrt{\frac{N}{2}\left(\frac{N}{2}+1\right) - m(m-1)}\delta_{l,m-1}\right)}{\Delta(m-l) + U(m^2 - l^2)} = \langle l|S|m\rangle.} \tag{19}$$

References

[1] W. Ketterle, D.S. Durfee, and D.M. Stamper-Kurn. *Making, probing and understanding Bose-Einstein condensates*. *arXiv* , (1999). DOI: 10.48550/ARXIV.COND-MAT/9904034.

[2] I. Bloch, J. Dalibard, and W. Zwerger. *Many-body physics with ultracold gases*. *Rev. Mod. Phys.* **80**, 885–964 (2008). DOI: 10.1103/RevModPhys.80.885.

[3] S. N. Bose. *Plancks Gesetz und Lichtquantenhypothese*. *Z. Physik.* **26**, 178–181 (1924). DOI: 10.1007/BF01327326.

[4] A. Einstein. *Quantentheorie des einatomigen idealen gases. zweite abhandlung*. *Albert Einstein: Akademie-Vorträge: Sitzungsberichte der Preußischen Akademie der Wissenschaften 1914–1932* , 245 - 257 (2005). DOI: 10.1002/3527608958.ch28.

[5] M. H. Anderson, *et. al. Observation of Bose-Einstein condensation in a dilute atomic vapor*. *Science* **269**, 198-201 (1995). DOI: 10.1126/science.269.5221.198.

[6] K. B. Davis, *et. al. Bose-Einstein condensation in a gas of sodium atoms*. *Phys. Rev. Lett.* **75**, 3969 (1995). DOI: 10.1103/PhysRevLett.75.3969.

[7] C. C. Bradley, C. A. Sackett, J. J. Tollett, and R. G. Hulet. *Evidence of Bose-Einstein condensation in an atomic gas with attractive interactions*. *Phys. Rev. Lett.* **75**, 1687 (1995). DOI: 10.1103/PhysRevLett.75.1687.

[8] T. Pudlik. *The open Bose-Hubbard dimer*. *OpenBU* (2016). https://hdl.handle.net/2144/19214.

[9] P. Zoller, J.I. Cirac, L. Duan, and J.J. García-Ripoll. *Course 4 - Quantum Optical Implementation of Quantum Information Processing*. *Elsevier.* **79**, 187-189, 191-222 (2004). DOI: https://doi.org/10.1016/S0924-8099(03)80028-8.

[10] I. Bloch, and P. Zoller. *Chapter 5 - Ultracold Atoms and Molecules in Optical Lattices*. *Elsevier.* **5**, 121-156 (2012). DOI: https://doi.org/10.1016/B978-0-444-53857-4.00005-2.

[11] S. Raghavan, A. Smerzi, S. Fantoni, and S. R. Shenoy. *Coherent oscillations between two weakly coupled Bose-Einstein condensates: Josephson effects, π oscillations, and macroscopic quantum self-trapping*. *Phys. Rev. A.* **59**, 620 (1999). DOI: 10.1103/PhysRevA.59.620.

[12] M. P. A. Fisher, P. B. Weichman, G. Grinstein, and D. S. Fisher. *Boson localization and the superfluid-insulator transition*. *Phys. Rev. B.* **40**, 546 (1989). DOI: 10.1103/PhysRevB.40.546.

[13] A. Giraldo, *et. al. The driven-dissipative Bose–Hubbard dimer: phase diagram and chaos*. *New J. Phys.* **22**, 043009 (2020). DOI: 10.1088/1367-2630/ab7539.

[14] A. Polkovnikov, S. Sachdev, and S. M. Girvin. *Nonequilibrium Gross-Pitaevskii dynamics of boson lattice models*. *Phys. Rev. A.* **66**, 053607 (2002). DOI: 10.1103/PhysRevA.66.053607.

[15] H. Hennig, J. Dorignac, and D. K. Campbell. *Transfer of Bose-Einstein condensates through discrete breathers in an optical lattice*. *Phys. Rev. A.* **82**, 053604 (2010). DOI: 10.1103/PhysRevA.82.053604.

[16] H. Hennig, and R. Fleischmann. *Nature of self-localization of Bose-Einstein condensates in optical lattices*. *Phys. Rev. A.* **87**, 033605 (2013). DOI: 10.1103/PhysRevA.87.033605.

[17] M. Albiez, *et. al. Direct Observation of Tunneling and Nonlinear Self-Trapping in a Single Bosonic Josephson Junction*. *Phys. Rev. Lett.* **95**, 010402 (2005). DOI: 10.1103/PhysRevLett.95.010402.

[18] T. Zibold, E. Nicklas, C. Gross, and M. K. Oberthaler. *Classical Bifurcation at the Transition from Rabi to Josephson Dynamics*. *Phys. Rev. Lett.* **105**, 204101 (2010). DOI: 10.1103/PhysRevLett.105.204101.

[19] A. Tomadin. *Quantum chaos with ultracold atoms in optical lattices*. (2006).

[20] T. Pudlik, H. Hennig, D. Witthaut, and D. K. Campbell. *Dynamics of entanglement in a dissipative Bose-Hubbard dimer*. *Phys. Rev. A* **88**, 063606 (2013). DOI: 10.1103/PhysRevA.88.063606.

[21] M. R. Andrews, *et. al. Observation of Interference Between Two Bose Condensates*. *Science* **275**, 637-641 (1997). DOI: 10.1126/science.275.5300.637.

[22] M. R. Matthews, *et. al. Vortices in a Bose-Einstein Condensate*. *Phys. Rev. Lett.* **83**, 2498 (1999). DOI: 10.1103/PhysRevLett.83.2498.

[23] C. Becker, *et. al. Oscillations and interactions of dark and dark–bright solitons in Bose–Einstein condensates*. *Nature Physics.* **4**, 496-501 (2008). DOI: 10.1038/nphys962.

[24] D. Jaksch, C. Bruder, J. I. Cirac, C. W. Gardiner, and P. Zoller *Cold Bosonic Atoms in Optical Lattices*. *Phys. Rev. Lett.* **81**, 3108 (1998). DOI: 10.1103/PhysRevLett.81.3108.

[25] Fisher, M. P. A., Weichman, P. B., Grinstein, G., and Fisher, D. S. *Boson localization and the superfluid-insulator transition.*. *Phys. Rev. B,* **40**, 546. (1989). DOI: 10.1103/physrevb.40.546.

[26] Bloch, I., Dalibard, J., and Nascimbène, S. *Quantum simulations with ultracold quantum gases. Nature Physics,* **8**, pages 267–276. (2012). DOI: 10.1038/nphys2259.

[27] Greiner, M., Mandel, O., Esslinger, T., Hänsch, T. W., and Bloch, I. *Quantum phase transition from a superfluid to a Mott insulator in a gas of ultracold atoms. Nature Physics,* **415**, 39-44. (2002). DOI: 10.1038/415039a.

[28] Weitenberg, C. *Single-Atom Resolved Imaging and Manipulation in an Atomic Mott Insulator. Dissertation, LMU München: Faculty of Physics* (2011). DOI: 10.5282/edoc.13425.

[29] Endres, M. *Probing correlated quantum many-body systems at the single-particle level. Dissertation, LMU München: Faculty of Physics* (2013). DOI: 10.5282/edoc.15506.

[30] Hubbard J. *Electron correlations in narrow energy bands. Proceedings of the Royal Society A: Mathematical, Physical and Engineering Sciences,* **276**, 238–257. (1963). DOI: 10.1098/rspa.1963.0204.

[31] Ashcroft, N.W. and Mermin, N.D. *Solid State Physics. Saunders College, Philadelphia,* **116, 217.**, pages . (1976).

[32] Trotzky S., Pollet L., Gerbier F., Schnorrberger U., Bloch I., Prokofev N. V., Svistunov B., and Troyer M. *Suppression of the critical temperature for superfluidity near the Mott transition. Nature Phys.,* **6**, 998–1004. (2010). DOI: 10.1038/nphys1799.

[33] Morsch O. and Oberthaler M. *Dynamics of Bose-Einstein condensates in optical lattices. Rev. Mod. Phys.,* **78**, 179. (2006). DOI: 10.1103/RevModPhys.78.179.

[34] Glück M., Kolovsky A. R., Korsch H. J., and Zimmer F. *Wannier-Stark resonances in semiconductor superlattices. Phys. Rev. B* **65**, 115302. (2002). DOI: 10.1103/PhysRevB.65.115302.

[35] Muñoz-Arias M.H, Madroñero J., and Parra-Murillo C. A. *Off-resonant many-body quantum carpets in strongly tilted optical lattices. Phys. Rev. A* **93**, 043603. (2016). DOI: 10.1103/PhysRevA.93.043603.

[36] Kolovsky A. R. and Buchleitner A. *Floquet-Bloch operator for the Bose-Hubbard model with static field. Phys. Rev. E* **68**, 056213. (2003). DOI: 10.1103/PhysRevE.68.056213.

[37] Parra-Murillo, C. A., Madroñero, J., and Wimberger, S. *Exact numerical methods for a many-body Wannier–Stark system. Computer Physics Communications* **186**, 19-30. (2015). DOI: 10.1016/j.cpc.2014.09.008.

[38] Parra-Murillo, C. A., Madroñero, J., and Wimberger, S. *Two-band Bose-Hubbard model for many-body resonant tunneling in the Wannier-Stark system. Phys. Rev. A* **88**, 032119. (2013). DOI: 10.1103/PhysRevA.88.032119.

[39] Longhi, S. *Bloch oscillations and Wannier-Stark localization in a tight-binding lattice with increasing intersite coupling. Phys. Rev. B* **80**, 033106. (2009). DOI: 10.1103/PhysRevB.80.033106.

[40] Guo, X., Ge, Z., Li, H., Wang, Z., Zhang, Y., Song, P., Xiang, Z., Song, X., Jin, Y., Lu, L., Xu, K., Zheng, D., and Fan, H. *Observation of Bloch oscillations and Wannier-Stark localization on a superconducting quantum processor. Npj Quantum Information* **7**, 1-6. (2021). DOI: 10.1038/s41534-021-00385-3.

[41] Wilkinson S. R., Bharucha C. F., Madison K. W., Qian Niu, and Raizen M. G. *Observation of Atomic Wannier-Stark Ladders in an Accelerating Optical Potential. Phys. Rev. Lett.* **76**, 4512. (1996). DOI: 10.1103/PhysRevLett.76.4512.

[42] Zapata J., Guzmán A. M, Moore M. G., and Meystre P. *Gravity-induced Wannier-Stark ladder in an optical lattice. Phys. Rev. A* **63**, 023607. (2001). DOI: 10.1103/PhysRevA.63.023607.

[43] Andronov, A.A., Dodin, E.P., Zinchenko, D.I. *et al. Stimulated emission at transitions between Wannier–Stark ladders in semiconductor superlattices. Jetp Lett.* **102**, 207–211. (2015). DOI: 10.1134/S0021364015160031.

[44] Sobolev, M.M., Cirlin, G.É., Tonkikh, A.A. *et al. Wannier-stark effect in Ge/Si quantum dot superlattices. Semiconductors* **42**, 305–309. (2008). DOI: 10.1134/S1063782608030111.

[45] Smerzi, A., Fantoni, S., Giovanazzi, S., and Shenoy, S. R. *Quantum Coherent Atomic Tunneling between Two Trapped Bose-Einstein Condensates Phys. Rev. Lett.* **79(25)**, 4950–4953 ((1997). DOI: 10.1103/physrevlett.79.4950.

[46] Auerbach, A., Arovas, D.P. *Schwinger Bosons Approaches to Quantum Antiferromagnetism. In: Lacroix, C., Mendels, P., Mila, F. (eds) Introduction to Frustrated Magnetism. Springer Series in Solid-State Sciences,* **vol 164.** Pages 365-377, Springer, Berlin, Heidelberg. (2010). DOI: 10.1007/978-3-642-10589-0_14.

[47] Pappalardi, Silvia. *Entanglement dynamics and chaos in long-range quantum systems. Dissertation, SISSA Trieste: THEORY and NUMERICAL SIMULATIONS of CONDENSED MATTER* (2020). https://hdl.handle.net/20.500.11767/114415.

[48] Hillery, M., Zubairy, M. S. *Entanglement Conditions for Two-Mode States Phys. Rev. Lett.* **96**, 050503 (2006). DOI: 10.1103/PhysRevLett.96.050503.

[49] Bravyi, S., DiVincenzo, D. P., Loss, D. *Schrieffer–Wolff transformation for quantum many-body systems Ann. Phys.* **326(10)**, 2793–2826 (2011). DOI: 10.1016/j.aop.2011.06.004.